ASTRONOMY & ASTROPHYSICS
SUPPLEMENT SERIES

Astron. Astrophys. Suppl. Ser. **98,** 477-504 (1993)

New dating of galactic open clusters

G. Meynet[1], J.-C. Mermilliod[2] and A. Maeder[1]

[1] Geneva Observatory, Ch. des Maillettes 51, CH-1290 Sauverny, Switzerland
[2] Institut d'Astronomie de l'Université de Lausanne, Ch. des Maillettes 51, CH-1290 Sauverny, Switzerland

Received June 16; accepted August 6, 1992

Abstract. — A new set of isochrones for solar metallicity computed from models taking into account mass loss and moderate overshooting and using the recent opacity tables by Rogers & Iglesias (1992) has been used to determine the ages of 30 galactic open clusters covering an interval of age from 4 10^6 to 9.5 10^9 years. The clusters collected here constitute an ensemble of homogeneous and accurate data, well discussed for distance, reddening, membership and binarity, and thus they provide a basic reference for age determinations. The present set of isochrones remarkably well fits the observed colour-magnitude diagrams of the clusters and may thus be expected to provide reliable ages. Analytic relations between several characteristics of the isochrones and the age are given and can be used for further age calibrations consistent with this homogeneous scale. The evolutionary tracks and isochrones used in this work are available on request.

Key words: clusters: open, and association — stars: evolution of — stars: Hertzsprung — Russell diagram — stars: population I — stars: structure of

1. Introduction

The ages of the galactic clusters play a central role in many astrophysical problems. Among them we can quote the estimate of an inferior limit for the age of the galactic disk (Grenon 1990), the study of the OB associations in relation with the process of sequential star formation (Blaauw 1991), the determination of the maximum initial mass for the formation of the white dwarfs (Weidemann 1990), or the study of stellar rotation decay with time (Barry 1988). So far ages of open clusters have been estimated with various methods and were based on different grids of models. Consequently, it may be difficult to order correctly open clusters in a sequence of increasing age by using the published data. To overcome this problem, it is important that open cluster ages are based on the same grid of models and determined in a homogeneous way.

The age determination is best performed by fitting an isochrone to the cluster colour-magnitude diagram. This requires however a lot of observational data of good quality and, in the best case, the knowledge of membership and binarity. To overcome this drawback, several statistical methods have been developed in the past. Lindoff (1968) defined a normalised parameter Γ_{25} which he linked to age. Harris (1976) used the parameter A_{12} formed by the two brightest stars in the cluster. Taff and Littleton (1973) investigated the relation between the $(B-V)_0$ colour index of the second brightest star in the cluster and age. Mermilliod (1981) gave an analytical relation between the bluest $(B-V)_0$ and $(U-B)_0$ colours and the age. More references about the different methods used to determine the age of the open clusters may be found in the introduction of Lindoff (1968).

The first aim of this work is to test the capacity of the new grids of stellar models computed by Schaller et al. (1992) with up to date physical ingredients, to reproduce the observed sequences of open clusters covering the widest possible interval of ages. Then this homogeneous set of theoretical isochrones and the facility offered by the database on stars in open clusters (Mermilliod 1988, 1992) will be used to provide new age determinations for the best studied open clusters in the solar neighbourhood.

The models used to compute the present set of isochrones are those by Schaller et al. (1992) for Pop. I abundances with $(X, Y, Z) = 0.68, 0.30, 0.02$. Details about the various physical ingredients of the stellar models are given in that paper. Let us just mention that the new radiative opacities by Rogers and Iglesias (1992) have been used. The changes with respect to the Los Alamos 1977 opacities are quite large: they typically amount to a factor 3 at 300000 K for solar metallicity. For the mass loss rates the general procedure described by Maeder (1990) was followed. Namely, the mass loss rates $\dot{M}$ are given by

Send offprint requests to: G. Meynet

de Jager et al. (1988; cf. also Nieuwenhuijzen & de Jager 1991) for stars throughout the HR diagram except the WR stars. In this last case a $\dot{M}$ vs mass relation found by Langer (1989ab) for WNE and WC stars was adopted. For WNL, the average mass loss rate of 4 $10^{-5} M_{\odot}$ per year was taken (cf. Conti 1988). The amount of overshooting from the convective cores is characterized by a distance of overshooting $d_{\rm over} = 0.20 H_{\rm p}$, where $H_{\rm p}$ is the pressure scale height at the edge of the classical core. This value for the overshooting parameter is slightly reduced compared to the one given by Maeder & Meynet (1989) who used the Los Alamos Opacity Library (cf. Huebner et al. 1977). The algorithms used for the computation of chemical changes have been improved to treat more accurately convective cores, particularly when overshooting is significant. This leads to a reduction of some timescales with respect to those given in Maeder and Meynet (1989) (see Sect. 2.1 below).

The isochrones are described in Sect. 2. In Sect. 3 theoretical calibrations and analytic relations are presented. Comparison with stellar observations are performed in Sect. 4.

2. Description of the isochrones

The grid of evolutionary models from 0.8 to $120 M_{\odot}$ for solar metallicity (Schaller et al. 1992) has been used to compute isochrones in the range $6.5 \leq \log t \leq 10.1$. The isochrones in the theoretical plane $\log L/L_{\odot}$, $\log T_{\rm eff}$ are represented in Fig. 1 and in the observational one (M_v, $(B-V)_0$) in Fig. 2. For logarithms of the age, $\log t$, superior or equal to 9.6, we have plotted the isochrones computed from models without overshooting. We can note the change of the width of the main sequence (MS) in the transition region.

The calibrations necessary to transfer the isochrones from the theoretical plane ($\log L/L_{\odot}$, $\log T_{\rm eff}$) to the observational ones (M_v,$(B-V)_0$), (M_v,$(U-B)_0$) are the same as in Maeder and Meynet (1991) at the exception of the relation $(B-V)_0$ vs $\log T_{\rm eff}$ for main sequence stars of effective temperatures between 5000 and 8000 K, which was taken from Arribas & Martinez Roger (1988).

2.1. *Effects of the new opacities*

In Fig. 3 are superposed the isochrones for $\log t =$ 6.5, 7.0, 7.5, 8.0, 8.5, 9.6 and 10.0 computed from models using the Los Alamos opacities (dashed lines, Maeder & Meynet 1991) and those from the new grid (solid lines). A detailed comparison of the evolutionary tracks on which these two sets of isochrones are based may be found in Schaller et al. (1992). Concerning the isochrones the following comments may be made:

1) The present main sequence isochrones for $\log t < 9.0$ are slightly displaced to the red with respect to the previous ones. Moreover they are at a little lower luminosity. The higher opacities used in this work are mainly responsible for these differences which have little effect on the age determinations.

2) The same reason may be invoked to explain the shortening of the blue loops which appear along the isochrones corresponding to ages in the range $7.2 < \log t < 8.0$. We emphasize in Sect. 4 that these new results remarkably fit the observations.

3) We can see from Fig. 3 that the widths of the main sequences are in very good agreement except in the upper part of the HR diagram. This difference was already found by Stothers and Chin (1977, 1985) who have shown that an increase of the opacities in the outer layers of massive stars may produce a MS band covering all the HR diagram. We shall see below whether or not such a widening of the MS is supported by the observations.

4) The red giant branches (RGB) of the new isochrones are slightly displaced to the blue which enables this set of theoretical time-lines to better reproduce the observed RGB (see Figs. 36 to 38).

The changes in the age determinations due to the overshooting from convective cores have been discussed in Maeder & Meynet (1991). Let us just mention here that the inclusion of this physical ingredient in the models produce a greater age for a given cluster.

As mentioned in the introduction, an insufficiency in the numerical scheme led the models of 1.3 to $2.5 M_{\odot}$ computed with overshooting by Maeder & Meynet (1989) to have too long a timescale, although their structure was correct. In Fig. 4 the hydrogen burning lifetime for the two grids computed by Schaller et al. (1992) for metallicities equal to 0.020 and 0.001 are plotted in function of the initial masses (in logarithm) together with the results obtained by Maeder and Meynet (1989). We can see that the difference is significant on a short interval of masses between 1.3 and $2 M_{\odot}$, the amplitude of the discrepancy is of the same order than the difference in lifetimes between the two sets of models computed by Schaller et al. (1992) for $Z = 0.020$ and $Z = 0.001$. Finally we note that the old models computed without overshooting are in perfect agreement with the new ones.

2.2. *The lowest mass limits for models with overshooting*

This problem is discussed in some details in Maeder and Meynet (1991). Let us briefly recall here the main arguments. Comparisons with the observations (see Sect. 3) show that isochrones computed from models with a moderate overshooting are required to fit the observed cluster sequence of young and intermediate age clusters (age $\leq 2\ 10^9$ yr). For old clusters, like M67 with an age of $4\ 10^9$ yr, no evidence for overshooting is present, which is not surprising since for small stellar masses no convective core is expected and by consequence no overshooting

either. For ages inbetween, which correspond to masses at the top of the main sequence around $1.4M_\odot$, the size of the convective core diminishes very much to finally vanish near $1.2M_\odot$. The exact behaviour of the cores in this transition region is not known. In the absence of a satisfactory theoretical basis for the determination of the extension of the convective core in this mass range, it seems necessary to perform accurate comparisons between observed sequences and isochrones before making any age determination.

3. Analytic relations

The object of this section is to present theoretical relations between the age and some important values characteristic of the isochrones as for instance the effective temperature of the reddest point on the main sequence. *We emphasize that an age estimate is meaningful only when there is a complete excellent agreement in the comparison of the observed and theoretical sequence.*

Figure 5a presents the relation between the logarithm of the effective temperature at the blue and red turnoffs (BTO and RTO respectively) and the logarithm of the age. What we mean by BTO and RTO is indicated in Fig. 3. At a given age, the $T_{\rm eff}$ of the RTO is essentially independent of overshooting. This makes this feature $T_{\rm eff}$ (RTO) a most valuable age indicator. On the contrary the $T_{\rm eff}$ of the bluest point on the isochrones in the main sequence, which is frequently used for age determination, is very sensitive to overshooting (Maeder & Meynet 1991). From Fig. 5a we can see that the curve corresponding to the RTO deviates from the one for the BTO for log age < 7.1. This is a consequence of the large widening of the main sequence for initial masses between 40 and $85M_\odot$.

The $(B-V)_0$ vs log *age* relations for the BTO and RTO are represented in Fig. 5b. Due to the linearity of the $\log T_{\rm eff}$ vs log *age* relation over a great part of the domain considered here (see Fig. 5a), this function has the same shape as the $(B-V)_0$ vs $\log T_{\rm eff}$ calibration. In particular the very low dependence of $(B-V)_0$ on $\log T_{\rm eff}$ at high temperatures, produces the flattening of the curve for log age ≤ 8.2. Figure 5c presents the $(U-B)_0$ vs log *age* calibration, which is useful for the youngest clusters, since this photometric index is more sensitive to the effective temperature and therefore to the age in this domain.

The absolute visual magnitude M_v at the RTO as a function of the age is presented in Fig. 5d. In Fig. 5e, M_v at the beginning of the blue loop (see Fig. 3) is given in function of the age. This relation is useful to estimate the age of an open cluster which presents a sufficiently well marked giant concentration. Evidently it should not be applied to clusters older than one billion years, in which the absolute magnitude of the clump is constant (clusters with stars having gone through the He-flash). Let us note that this calibration is in very good agreement with the semi-empirical one deduced by Mermilliod (1981).

The actual mass at the RTO is represented as a function of the logarithm of the age in Fig. 5f. Mass loss during the MS begins to become important only for stars having an initial mass superior to about $12M_\odot$. Therefore, the actual mass at the RTO for clusters with $\log t >\sim 7.2$ is equal to the initial one. This relation may be used to estimate a lower limit for the initial mass of the giants or supergiants in a cluster whose age has been determined by the present set of isochrones.

Nine analytic relations deduced from the theoretical calibrations presented in Figs. 5a to f are given in Table 1. In the first column is indicated the kind of the relation as well as the range of ages where it applies, the analytic expression is given in the second one, the domain of validity is presented in the third column. The last one gives the maximum absolute deviation between the values as obtained from the theoretical isochrones and those given by the analytic expressions.

In Tables 2 and 3 the predicted values for the actual mass, $M_{\rm ac}/M_\odot$, the initial mass, $M_{\rm in}/M_\odot$, $\log L/L_\odot$, $\log T$eff, $\log g$, $M_{\rm bol}$, M_v, $(B-V)_0$, and $(U-B)_0$ are expressed in function of the logarithm of the age for the BTO and RTO respectively.

4. Comparisons with the stellar observations

4.1. *Description of the observational sources*

The clusters presented in this work have been selected among the 500 objects contained in the database for stars in open clusters developed by one of us (Mermilliod 1988, 1992) under the following conditions: (1) the main sequence is well defined by the available photoelectric or CCD *UBV* data, (2) the influence of non-member stars on the definition of the upper main sequence and turnoff is negligible, (3) the chemical composition is nearly solar, (4) when many observational sources are available, the zero point differences on V and $B-V$ must be less than 0.05 and 0.02 respectively.

On the basis of condition (1) we have rejected many clusters because the few available photoelectric data were obtained for calibration purpose only. We did not try to use those clusters which would have required a complete analysis of the photometric membership, which is beyond the scope of the present paper (condition (2)). Condition (3) leads to the rejection of several clusters with interesting colour-magnitude diagrams, but non-solar chemical composition. For example, the Hyades and Praesepe have a metallicity higher than solar, while the anticenter clusters, like NGC 2204, 2243, 2420, 2506, are quite deficient. They will be used to test isochrones based on models with a different metal content which will be available in a near future. Condition (4) is also important to obtain accurate

age determination by isochrone fitting. The final sample contains 30 open clusters.

The data plotted are based either on mean *UBV* data or CCD (NGC 188, 2439, 2682 (M67), 6067, 6705 and 6791) observations. In the case of IC 4651, we preferred the very good photographic data published by Anthony-Twarog et al. (1988) to the incomplete photoelectric or CCD data, because they produce a better defined sequence. The membership of the red giants has been confirmed by radial velocity observations obtained, for most clusters, with the Coravel scanners. Those for NGC 2682 (M67) and 6705 (M11) have been published by Mathieu et al (1986). No data are yet available for NGC 188, 2355 and 6791. The individual data and references for each cluster can be obtained from one of the authors (J.-C. M.) by E-mail (mermio@scsun.unige.ch).

4.2. *General overview of the observational set of data*

The synthetic colour-magnitude diagram obtained by the superposition of all the clusters studied in the present work (more than 4000 stars) is presented in Fig. 6, with a few theoretical time-lines superposed. For $(B-V)_0 > 1.00$, the main sequence is mostly based on that of the Pleiades.

One of the most striking feature of this plot is the concentration of red giants along a curved line which approximately follows the bottom of the loops ($2 \geq M_v \geq -3$). We can note also that the width of the main sequence (~ 0.75 mag.) is dominated by the binaries. The tops of the main sequences are well visible particularly for the old clusters.

4.3. *Theoretical fits of the observed colour-magnitude diagrams and age determination*

The comparisons of the isochrones and the clusters are displayed in Figs. 9 to 38 and are ordered by increasing age. Table 4 gives for each cluster, the distance–modulus, reddening value and resulting age as well as the number of the figure where it is displayed. The distance-modulus determination is based on the fitting of a theoretical ZAMS deduced from the present grid.

Many observational features are very well reproduced by the present set of isochrones:

1) The morphology of the blue envelope of the MS stars. We note that, in general, the curvature of the theoretical isochrone is slightly more pronounced than for the observed sequence. Such an effect is just that expected from the presence of unresolved binary stars. This can be seen in Figs. 7 and 8, where for illustrative purpose, the theoretical envelope of equal mass binaries and the usual isochrone are superposed to the colour magnitude diagrams of NGC 2287 and NGC 2355 respectively.

2) The terminal point of the MS is quite well reproduced. This well supports the hypothesis that some moderate overshooting is present. However for the very young Orion cluster, the theory predicts a much too bright absolute magnitude for the end of the MS (M_v=-7.9, see Table 3 and Fig. 9). This seems to indicate a narrower main sequence than that predicted by the models for this age. Interestingly enough, models with higher mass loss rates would lead to narrower MS for large masses (cf. Maeder 1981) and better agreement with the observations. Similar conclusions have been reached from WR luminosities by Schaller et al. (1992) and from WR abundances by Schaerer and Maeder (1992).

3) The positions of the red supergiants and the red giant branch are also correctly predicted by the present theoretical models. The apparition of the blue loops (for $\log age \geq 7.15$) along the isochrones well corresponds to the apparition of some blue supergiants in the observed colour-magnitude diagrams of the clusters. When the age increases the loops tend to be smaller, which is in good agreement with the observations (see Fig. 6).

We confirm the conclusion already reached by Maeder & Meynet (1991) concerning the lowest mass limits for models with overshooting. We see that the sequence of the old cluster M67 is better fitted by an isochrone without overshooting at an age of 4 10^9 yr (see Fig. 36). However the old cluster IC4651 is better fitted by an isochrone with overshooting at an age of 2 10^9 yr (see Fig. 35). This shows at which age the transition from one set of models to the other is likely to occur. In terms of mass, this corresponds to a transition located between 1.2 and $1.6 M_\odot$.

5. Conclusion

A new set of isochrones computed from models using the recent opacity tables from the Livermore group have been compared to the observed sequence of 30 galactic open clusters. For young and intermediate age clusters, very good overall agreement is obtained with isochrones computed with a moderate overshooting as given by $d_{over} = 0.20 H_p$. We do not find that differences due to opacities are such as to reduce the overshooting distance to zero, but we confirm that this phenomenon is likely very moderate (see also Stothers & Chin 1991ab).

The fits presented in Figs. 7 to 38 show that the present isochrones well agree with observations and may thus be expected to provide reliable ages. Therefore new datings have been obtained for galactic open clusters covering a broad range of ages.

More CCD observations of old clusters are needed to replace the old photographic data. The latter produce sequences which present too much scatter and therefore can not be used to constrain the models. In a near future it will also be possible to have information about the way the chemical abundances at the surface vary along a cluster's sequence. This will give very interesting constraints on

stellar models. Asteroseismology, applied in the context of a stellar cluster, will also provide very deep insights in stellar structure.

Acknowledgements. It is a pleasure to thank Dr J.-J. Claria (Cordoba, Argentina) for sending us a copy of his unpublished observations on NGC 5460 and the permission to use them. This work has been supported by continuous grants from the Swiss National Foundation for Scientific Research (FNRS).

References

Anthony-Twarog B.J., Mukherjee K., Caldwell N., Twarog B.A. 1988, AJ 95, 1453
Arribas, S., Martinez Roger, C. 1988, A&A 206, 63
Barry D.C. 1988, ApJ 334, 436
Blaauw A. 1991, In: Lada C.J., Kylafis N.D. (eds.) The Physics of Star Formation and Early Stellar Evolution NATO ASI Series Vol. 342, p. 125
Böhm–Vitense E. 1981, ARA&A, 19, 295
Conti P.S. 1988, In: Conti P.S., Underhill A.B. (eds) O-stars and Wolf-Rayet stars, NASA SP-497, p. 81
de Jager C., Nieuwenhuijzen H., van der Hucht K.A. 1988, A&AS 72, 259
Grenon M. 1990, In: Vangioni-Flam E., Cassé M., Audouze J., Tran Thanh Van J. (eds) Astrophysical Ages and Dating Methods, Editions Frontières, p. 153
Harris G.L.H. 1976, ApJS 30, 451
Huebner W.F., Merts A.L., Magee N.H.Jr., Argo M.F. 1977, Astrophysical Opacity Library, UC-34b
Kudritzki R.P., Hummer D.G. 1986, In: de Loore C., Willis A.J., Laskarides P. (eds) Luminous Stars and Associations in Galaxies, IAU Symp. 116, p.3
Langer, N. 1989a, A&A 210, 93
Langer, N. 1989b, A&A 220, 135
Lindoff U. 1968, Ark. Astr. 5, 1
Maeder A. 1981, A&A 102, 401
Maeder A. 1990, A&AS 84, 139
Maeder A., Meynet G. 1989, A&A 210, 155
Maeder A., Meynet G. 1991, A&AS 89, 451
Mathieu R.D., Latham D.W., Griffin R.F., Gunn J.E. 1986, AJ 92, 1100
Mermilliod J.-C. 1981, A&A 97, 235
Mermilliod J.-C. 1988, Bull. Inform. CDS 35, 77
Mermilliod J.-C. 1992, Bull. Inform. CDS 40, 115
Nieuwenhuijzen H., de Jager C. 1990, A&A 231, 134
Rogers F.J., Iglesias C.A. 1992, ApJS 79, 507
Schaerer, D., Maeder, A. 1992, A&A (submitted)
Schaller G., Schaerer D., Meynet G., Maeder A. 1992, A&A (in press)
Stothers R.B. 1991, ApJ 383, 820
Stothers R.B., Chin C.-W. 1977, ApJ 211, 189
Stothers R.B., Chin C.-W. 1985, ApJ 292, 222
Stothers R.B., Chin C.-W. 1991, ApJ 381, L67
Taff L.G., Littleton J.E. 1973, Astrophys. Letters 13, 133
Twarog B.A., Anthony–Twarog B.J. 1989 , AJ 97, 759
Weidemann V. 1990, ARA&A 28, 103

Table 1.

ANALYTIC RELATIONS

Relations	Analytic Expressions	Range of Validity	Precision
log (age) vs log T_{eff}	• log (age) = -3.499 log $T_{eff_{bt}}$ + 22.476	log $T_{eff_{bt}}$ ∈ [4.25 ; 4.56]	< 3 10^{-3}
at the BTO	• log (age) = -3.611 log $T_{eff_{bt}}$ + 22.956	[3.98 ; 4.25]	< 3 10^{-3}
log (age) ∈ [6.6 ; 9.6]	• log (age) = 15.142 (log $T_{eff_{bt}}$)^2 − 122.810 log $T_{eff_{bt}}$ + 257.518	[3.79 ; 3.98]	< 40 10^{-3}
log (age) vs log T_{eff}	• log (age) = -0.216 (log $T_{eff_{rt}}$)^2 − 2.990 log $T_{eff_{rt}}$ + 24.199	log $T_{eff_{rt}}$ ∈ [4.28 ; 4.41]	< 40 10^{-3}
at the RTO	• log (age) = -3.477 log $T_{eff_{rt}}$ + 22.304	[3.88 ; 4.28]	< 6 10^{-3}
log (age) ∈ [6.8 ; 9.6]	• log (age) = 66.801 (log $T_{eff_{rt}}$)^2 − 518.817 (log$T_{eff_{rt}}$) + 1016.140	[3.77 ; 3.88]	< 90 10^{-3}
log (age) vs (B-V)	• log (age) = 8.060 $(B-V)_{bt}$ + 9.208	$(B-V)_{bt}$ ∈ [-0.32 ; -0.18]	< 45 10^{-3}
at the BTO	• log (age) = -14.368 $(B-V)^2_{bt}$ + 1.861 (B-V) + 8.589	[-0.18 ; 0.00]	< 20 10^{-3}
log (age) ∈ [6.6 ; 9.6]	• log (age) = 1.726 $(B-V)_{bt}$ + 8.604	[0.00 ; 0.35]	< 30 10^{-3}
	• log (age) = 2.387 $(B-V)_{bt}$ + 8.365	[0.35 ; 0.52]	< 15 10^{-3}
log (age) vs (B-V)	• log (age) = 8.696 $(B-V)_{rt}$ + 9.252	$(B-V)_{rt}$ ∈ [-0.26 ; -0.17]	< 30 10^{-3}
at the RTO	• log (age) = -12.434 $(B-V)^2_{rt}$ + 1.876 $(B-V)_{rt}$ + 8.461	[-0.17 ; -0.03]	< 15 10^{-3}
log (age) ∈ [7.0 ; 9.6]	• log (age) = 1.805 $(B-V)_{rt}$ + 8.452	[-0.03 ; 0.19]	< 20 10^{-3}
	• log (age) = 4.400 $(B-V)^2_{rt}$ − 1.295 $(B-V)_{rt}$ + 8.889	[0.19 ; 0.57]	< 40 10^{-3}
log (age) vs (U-B) at BTO	• log (age) = -1.603 $(U-B)^2_{bt}$ − 0.970 $(U-B)_{bt}$ + 7.625	$(U-B)_{bt}$ ∈ [-1.16 ; -0.79]	< 40 10^{-3}
log (age) ∈ [6.6 ; 8.6]	• log (age) = -0.999 $(U-B)^2_{bt}$ + 0.692 $(U-B)_{bt}$ + 8.578	[-0.79 ; 0.01]	< 35 10^{-3}
log (age) vs (U-B)	• log (age) = 2.331 $(U-B)_{rt}$ + 9.141	$(U-B)_{rt}$ ∈ [-0.92 ; -0.57]	< 20 10^{-3}
at the RTO	• log (age) = 1.317 $(U-B)_{rt}$ + 8.556	[-0.57 ; -0.27]	< 15 10^{-3}
log (age) ∈ [7.0 ; 8.6]	• log (age) = 1.940 $(U-B)^2_{rt}$ + 1.554 $(U-B)_{rt}$ + 8.476	[-0.27 ; -0.07]	< 30 10^{-3}
Actual mass at RTO	• log $(M/M_\odot)_{ac}$ = 0.337 (log (age))^2 − 5.509 log (age) + 23.278	log (age) ∈ [6.6 ; 7.6]	< 60 10^{-3}
vs log (age)	• log $(M/M_\odot)_{ac}$ = -0.411 log (age) + 3.980	[7.6 ; 8.4]	< 7 10^{-3}
	• log $(M/M_\odot)_{ac}$ = -0.342 log (age) + 3.396	[8.4 ; 9.6]	< 7 10^{-3}
log (age) vs M_v	• log (age) = 0.077 M_v + 7.205	M_v ∈ [-9.18 ; -6.57]	< 5 10^{-3}
at the RTO	• log (age) = 0.031 M_v^2 + 0.528 M_v + 8.848	[-6.57 ; -3.12]	< 20 10^{-3}
log (age) ∈ [6.5 ; 9.6]	• log (age) = 0.409 M_v + 8.775	[-3.12 ; -0.67]	< 25 10^{-3}
	• log (age) = 0.275 M_v + 8.685	[-0.67 ; 3.33]	< 25 10^{-3}
log (age) vs M_v beg. of blue loop	• log (age) = 0.277 M_v + 8.661	M_v ∈ [-5.21 ; 0.47]	< 25 10^{-3}
log (age) ∈ [7.2 ; 9.0]	• log (age) = 0.415 M_v + 8.604	[0.47 ; 0.95]	< 30 10^{-3}

Table 2. Data ta the Blue Turnoff

log *age*	$M_{ac}/M_\odot$	$M_{in}/M_\odot$	log $L/L_\odot$	log T_{eff}	log g	M_{bol}	M_v	$(B-V)_0$	$(U-B)_0$
9.6	1.2187	1.2187	0.4429	3.7863	4.1769	3.6426	3.7036	0.5191	0.0267
9.5	1.2668	1.2668	0.5049	3.7995	4.1847	3.4878	3.5186	0.4700	0.0055
9.4	1.3301	1.3301	0.5863	3.8103	4.1677	3.2843	3.2904	0.4299	-0.0117
9.3	1.4123	1.4123	0.6936	3.8218	4.1320	3.0159	3.0049	0.3926	-0.0061
9.2	1.5479	1.5479	0.8707	3.8348	4.0471	2.5733	2.5460	0.3518	0.0086
9.1	1.6319	1.6319	0.9598	3.8529	4.0531	2.3504	2.3104	0.2937	0.0410
9.0	1.8144	1.8151	1.1645	3.8743	3.9800	1.8387	1.7987	0.2224	0.0981
8.9	1.9611	1.9612	1.3069	3.8981	3.9667	1.4827	1.4592	0.1540	0.1000
8.8	2.1678	2.1678	1.4979	3.9237	3.9217	1.0052	1.0171	0.1081	0.0920
8.7	2.3371	2.3371	1.6318	3.9495	3.9236	0.6705	0.7479	0.0590	0.0572
8.6	2.5608	2.5608	1.8023	3.9758	3.8979	0.2442	0.3978	0.0046	0.0137
8.5	2.7847	2.7847	1.9532	4.0032	3.8932	-0.1330	0.1327	-0.0335	-0.0724
8.4	3.0386	3.0386	2.1108	4.0308	3.8836	-0.5269	-0.1269	-0.0638	-0.1785
8.3	3.3266	3.3266	2.2688	4.0587	3.8768	-0.9220	-0.3741	-0.0913	-0.2749
8.2	3.6241	3.6241	2.4154	4.0866	3.8788	-1.2884	-0.5831	-0.1143	-0.3594
8.1	3.9707	3.9707	2.5755	4.1145	3.8702	-1.6888	-0.8154	-0.1303	-0.4312
8.0	4.3495	4.3495	2.7254	4.1424	3.8715	-2.0634	-1.0157	-0.1478	-0.4922
7.9	4.7881	4.7881	2.8861	4.1703	3.8638	-2.4654	-1.2417	-0.1662	-0.5647
7.8	5.2636	5.2637	3.0375	4.1979	3.8639	-2.8439	-1.4511	-0.1778	-0.6112
7.7	5.8063	5.8065	3.1918	4.2250	3.8610	-3.2295	-1.6781	-0.1881	-0.6605
7.6	6.4123	6.4127	3.3488	4.2521	3.8555	-3.6220	-1.9180	-0.1989	-0.7054
7.5	7.0867	7.0875	3.5048	4.2795	3.8524	-4.0120	-2.1641	-0.2107	-0.7446
7.4	7.9783	7.9815	3.6816	4.3085	3.8429	-4.4541	-2.4558	-0.2236	-0.7869
7.3	8.9730	8.9793	3.8563	4.3375	3.8352	-4.8907	-2.7440	-0.2378	-0.8328
7.2	10.2040	10.2284	4.0359	4.3659	3.8250	-5.3397	-3.0455	-0.2499	-0.8947
7.1	11.5902	11.6375	4.2127	4.3943	3.8171	-5.7818	-3.3405	-0.2600	-0.9438
7.0	13.3572	13.4610	4.3983	4.4230	3.8081	-6.2457	-3.6383	-0.2750	-0.9975
6.9	15.6145	15.8115	4.5954	4.4519	3.7944	-6.7385	-3.9624	-0.2916	-1.0549
6.8	18.6216	18.9679	4.8066	4.4810	3.7759	-7.2666	-4.3320	-0.3014	-1.0850
6.7	22.3944	22.9074	5.0100	4.5096	3.7672	-7.7750	-4.6632	-0.3111	-1.1207
6.6	27.6219	28.3368	5.2177	4.5373	3.7616	-8.2942	-5.0105	-0.3206	-1.1554
6.5	33.9014	34.7995	5.4036	4.5650	3.7754	-8.7589	-5.3039	-0.3300	-1.1900

Table 3. Data at the Red Turnoff

log *age*	$M_{ac}/M_\odot$	$M_{in}/M_\odot$	log $L/L_\odot$	log T_{eff}	log g	M_{bol}	M_v	$(B-V)_0$	$(U-B)_0$
9.6	1.3151	1.3151	0.6089	3.7724	3.9883	3.2279	3.3271	0.5722	0.0681
9.5	1.4067	1.4067	0.7269	3.7800	3.9299	2.9326	3.0081	0.5426	0.0368
9.4	1.5211	1.5211	0.8795	3.7858	3.8344	2.5512	2.6134	0.5211	0.0276
9.3	1.6380	1.6380	1.0171	3.7932	3.7587	2.2072	2.2525	0.4936	0.0157
9.2	1.7670	1.7678	1.1604	3.8033	3.6886	1.8489	1.8711	0.4561	-0.0005
9.1	1.9095	1.9098	1.3099	3.8160	3.6238	1.4752	1.4714	0.4106	-0.0126
9.0	2.0593	2.0593	1.4503	3.8340	3.5880	1.1242	1.0980	0.3545	0.0076
8.9	2.2333	2.2333	1.6064	3.8589	3.5667	0.7340	0.6940	0.2738	0.0570
8.8	2.4189	2.4189	1.7579	3.8839	3.5499	0.3553	0.3216	0.1946	0.1000
8.7	2.6218	2.6218	1.9092	3.9112	3.5429	-0.0230	-0.0304	0.1274	0.0968
8.6	2.8521	2.8521	2.0714	3.9397	3.5311	-0.4284	-0.3786	0.0787	0.0730
8.5	3.0972	3.0972	2.2217	3.9687	3.5327	-0.8042	-0.6713	0.0194	0.0255
8.4	3.3858	3.3858	2.3864	3.9976	3.5225	-1.2161	-0.9758	-0.0268	-0.0525
8.3	3.6871	3.6871	2.5374	4.0269	3.5258	-1.5935	-1.2120	-0.0596	-0.1638
8.2	4.0259	4.0259	2.6967	4.0561	3.5211	-1.9917	-1.4585	-0.0889	-0.2663
8.1	4.4228	4.4228	2.8600	4.0853	3.5156	-2.4001	-1.7022	-0.1136	-0.3562
8.0	4.8518	4.8518	3.0184	4.1147	3.5150	-2.7960	-1.9216	-0.1304	-0.4315
7.9	5.3305	5.3307	3.1691	4.1436	3.5209	-3.1728	-2.1176	-0.1485	-0.4948
7.8	5.8861	5.8866	3.3309	4.1720	3.5154	-3.5773	-2.3430	-0.1673	-0.5692
7.7	6.5033	6.5042	3.4949	4.2001	3.5075	-3.9872	-2.5807	-0.1786	-0.6145
7.6	7.2197	7.2220	3.6629	4.2283	3.4975	-4.4072	-2.8371	-0.1893	-0.6667
7.5	8.1130	8.1201	3.8380	4.2568	3.4871	-4.8450	-3.1156	-0.2008	-0.7125
7.4	9.1378	9.1537	4.0162	4.2848	3.4725	-5.2904	-3.4150	-0.2130	-0.7521
7.3	10.4035	10.4529	4.1997	4.3100	3.4464	-5.7492	-3.7428	-0.2244	-0.7893
7.2	11.8253	11.9163	4.3785	4.3358	3.4262	-6.1962	-4.0580	-0.2370	-0.8302
7.1	13.7907	14.0097	4.5881	4.3581	3.3727	-6.7202	-4.4674	-0.2444	-0.8809
7.0	16.2824	16.7170	4.7989	4.3777	3.3124	-7.2471	-4.8895	-0.2584	-0.9159
6.9	19.4502	20.2211	5.0163	4.3955	3.2432	-7.7907	-5.3434	-0.2600	-0.9458
6.8	23.8183	25.1295	5.2423	4.4056	3.1455	-8.3558	-5.8514	-0.2644	-0.9633
6.7	30.4698	33.0001	5.4869	4.3848	2.9250	-8.9672	-6.5731	-0.2600	-0.9280
6.6	39.7583	45.6434	5.7615	4.2588	2.2617	-9.6537	-7.9141	-0.2016	-0.7153
6.5	53.0578	68.7856	6.0516	4.1670	1.7299	-10.3789	-9.1759	-0.1640	-0.5560

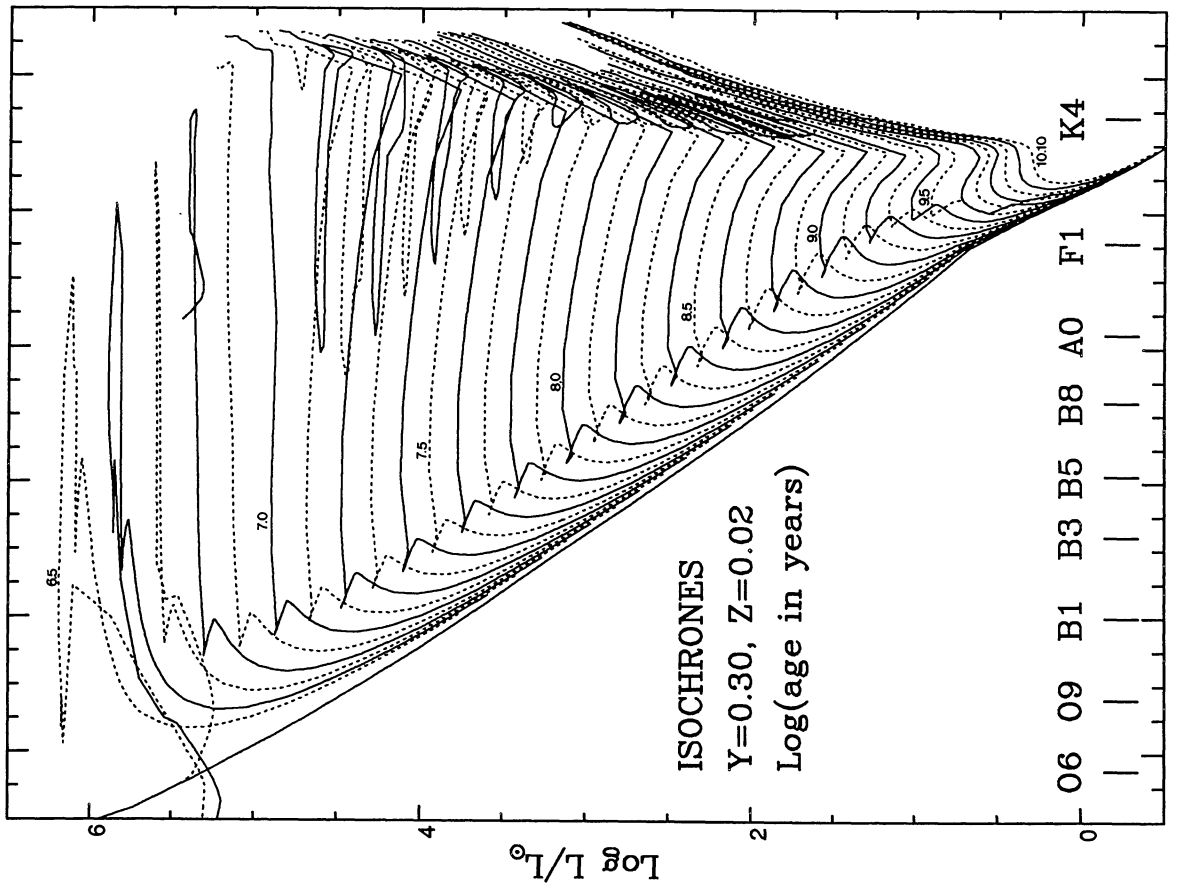

Fig. 1. The time–lines in the theoretical HR diagram for $\log t = 6.5$ to 10.1 are represented for each 0.1 dex in log *age*. The numbers indicate the logarithm of the age in years. The spectral types are taken from Kudritzki & Hummer (1986) and from Böhm-Vitense (1981). The isochrones are computed from models with a moderate overshooting, at the exception of those for log age ≥ 9.6 which are computed from models without overshooting

Table 4. Ages of the open clusters

Cluster	$m-M$	$E(B-V)$	log *age*	Fig.#
NGC 188	11.35	0.12	9.82	37
NGC 457	13.60	0.50	7.25	13
NGC 581	13.26	0.40	7.40	14
NGC 752	7.88	0.02	9.25	34
NGC 884	13.65	0.56	7.15	11
NGC 1039	8.65	0.10	8.25	25
NGC 1976	8.35	0.05	6.60	9
NGC 2287	9.15	0.01	8.38	28
NGC 2355	11.85	0.12	8.98	32
NGC 2360	10.40	0.08	9.00	33
NGC 2439	14.00	0.36	7.40	15
NGC 2516	8.35	0.12	8.15	21
NGC 2682	9.60	0.03	9.60	36
NGC 3532	8.35	0.04	8.50	31
NGC 4755	12.55	0.38	7.15	12
NGC 5460	9.50	0.12	8.20	22
NGC 5662	10.30	0.31	7.85	18
NGC 6025	9.95	0.16	8.10	23
NGC 6067	12.10	0.32	8.22	24
NGC 6087	10.30	0.20	7.85	19
NGC 6231	12.50	0.46	6.75	10
NGC 6242	11.45	0.39	7.70	16
NGC 6281	9.00	0.16	8.35	27
NGC 6475	7.08	0.06	8.35	26
NGC 6494	10.20	0.36	8.48	30
NGC 6705	12.70	0.40	8.40	29
NGC 6791	13.55	0.21	9.95	38
IC 4651	9.90	0.14	9.28	35
Alpha Per	6.36	0.09	7.72	17
Pleiades	5.60	0.04	8.00	20

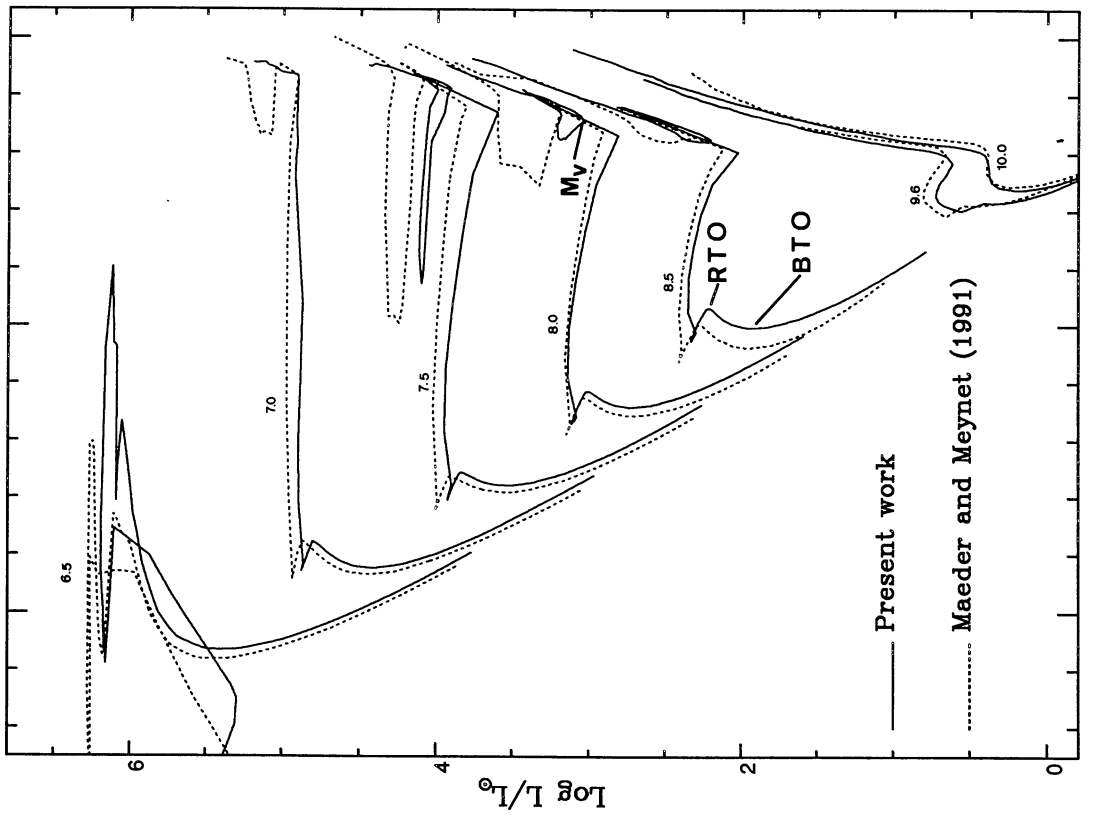

Fig. 3. Comparison of the isochrones computed with the opacities of Los Alamos (dashed lines, Maeder & Meynet 1991) and the ones derived from the new opacity tables from Rogers & Iglesias (1992) (solid lines, models from Schaller et al. 1992). For each pair the logarithm of the age is given. Are indicated also, on one of these isochrones, the positions of the red and blue turnoff, RTO and BTO respectively, as well as the magnitude M_v at the beginning of the blue loop; we refer to these particular positions in Fig. 5

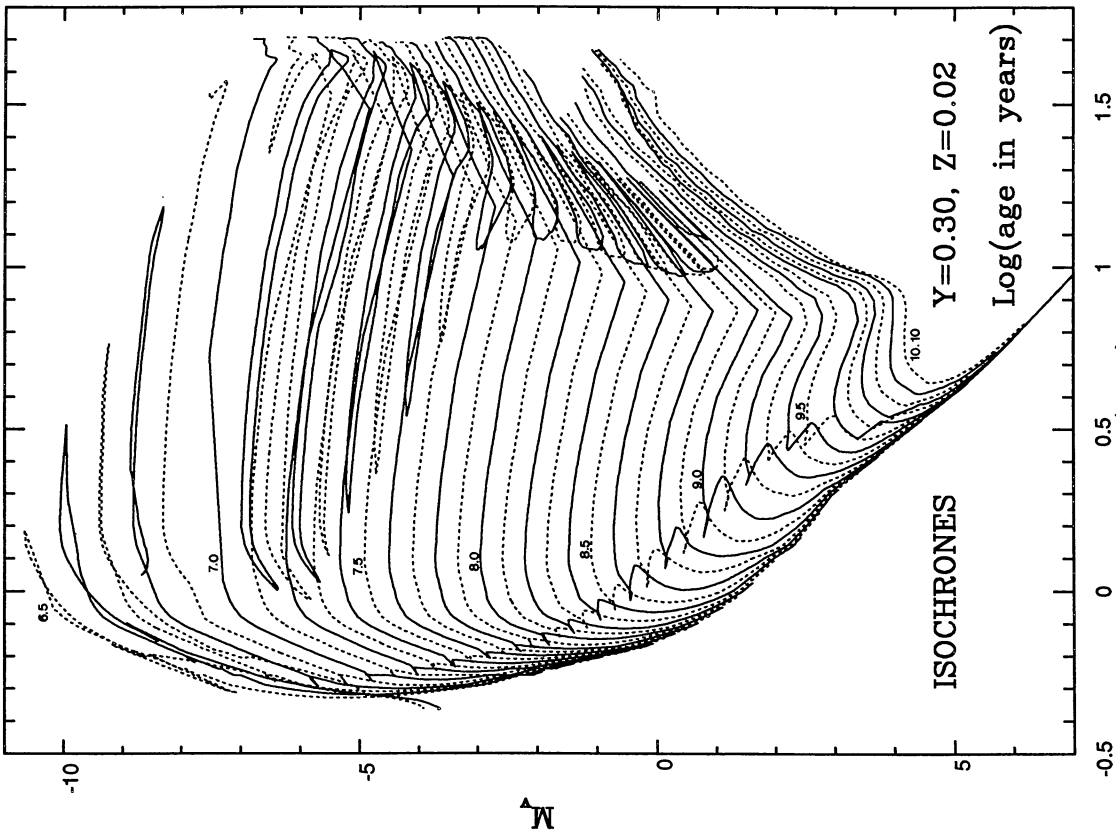

Fig. 2. Same as in Fig. 1 in the M_v versus $(B-V)_0$ plane. See the text about the calibrations used to transform the theoretical HR diagram to the observational one

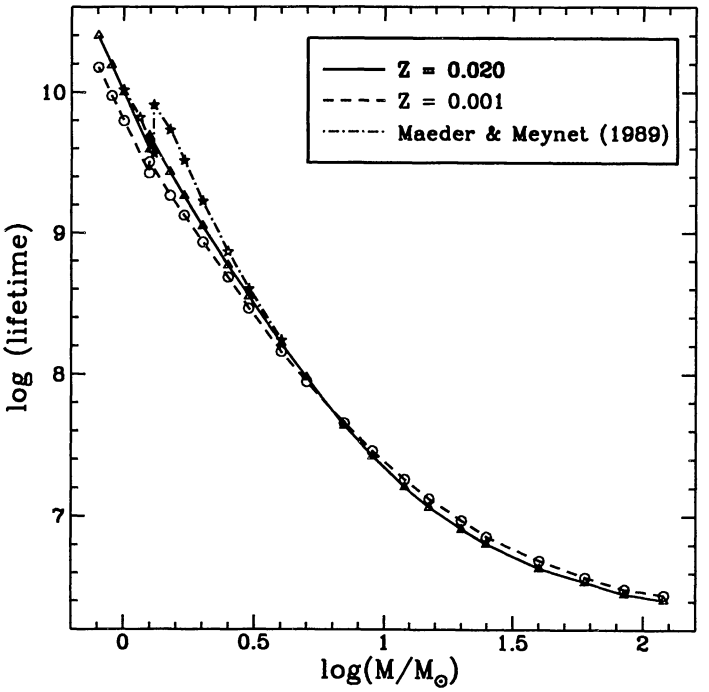

Fig. 4. The logarithm of the lifetimes in years for the H-burning phase are represented in function of the logarithm of the initial masses expressed in solar units, for the two sets of models at $Z = 0.020$ and $Z = 0.001$ computed by Schaller et al. (1992) and for the set of models computed by Maeder & Meynet (1989). The lifetimes for the models with and without overshooting are shown for the $1.25M_{\odot}$, in the case of Schaller's models, and for the $1.3M_{\odot}$ model in the case of Maeder & Meynet 's models

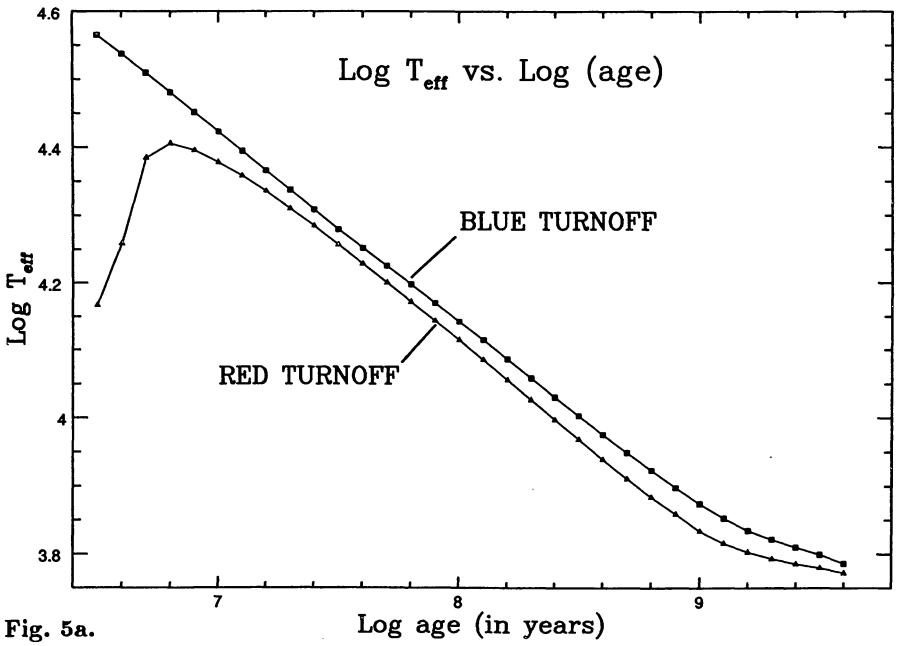

Fig. 5a.

Fig. 5. Various quantities as a function of the age, a) the effective temperature at the BTO and RTO, b) $(B-V)_0$ at the BTO and RTO, c) $(U-B)_0$ at the BTO and RTO, d) M_v at the RTO, e) M_v at the beginning of the blue loop, f) the actual mass at the RTO

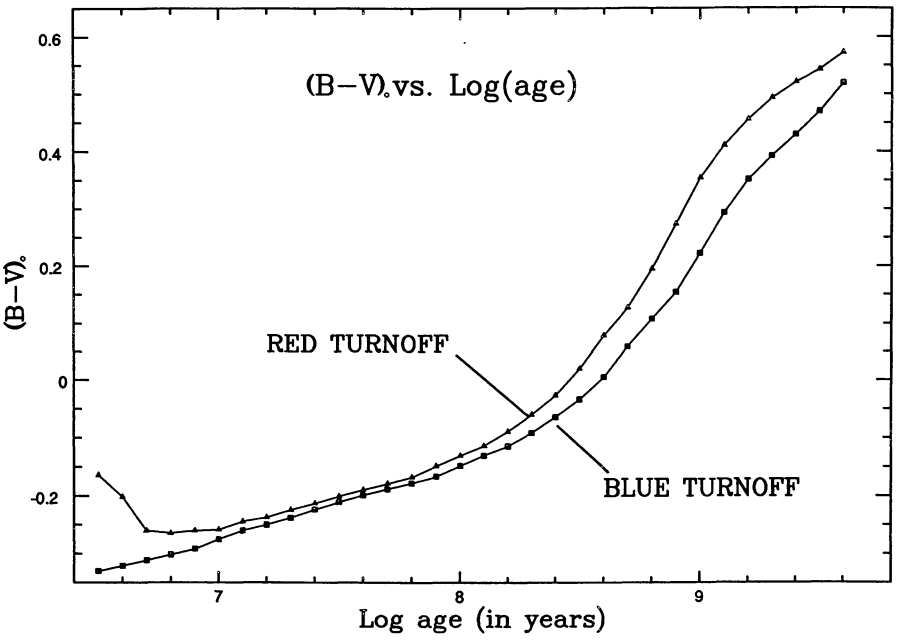

Fig. 5b.

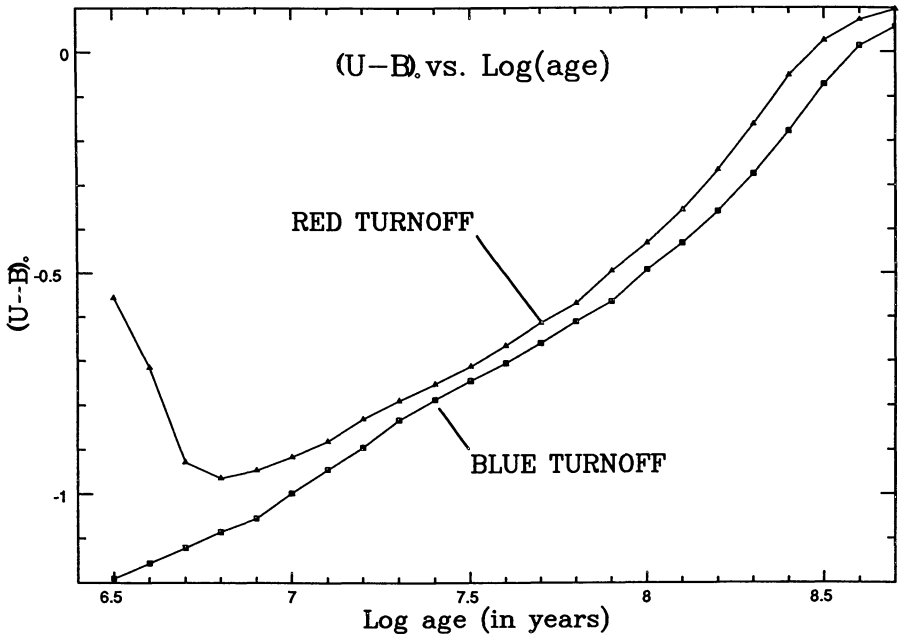

Fig. 5c.

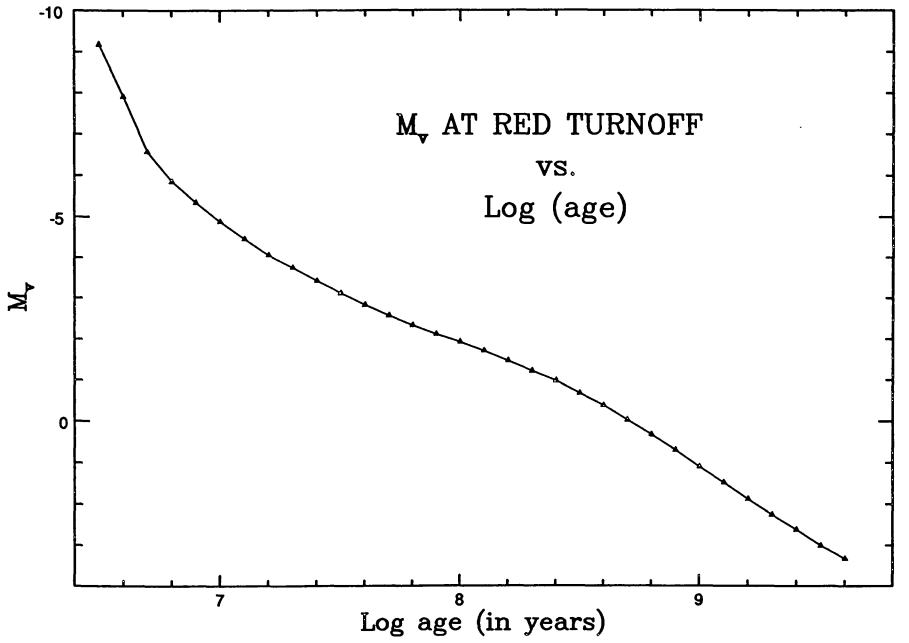

Fig. 5d.

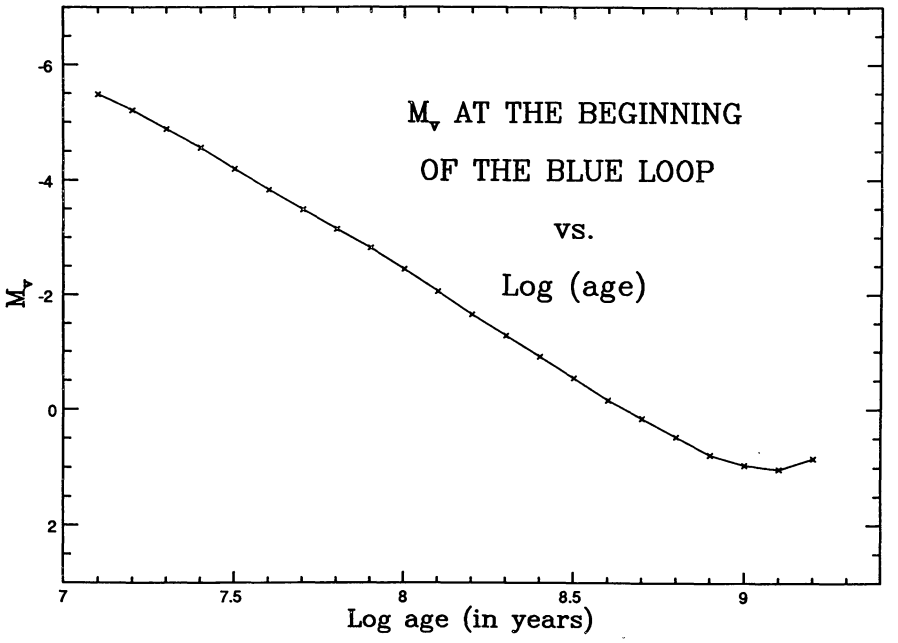

Fig. 5e.

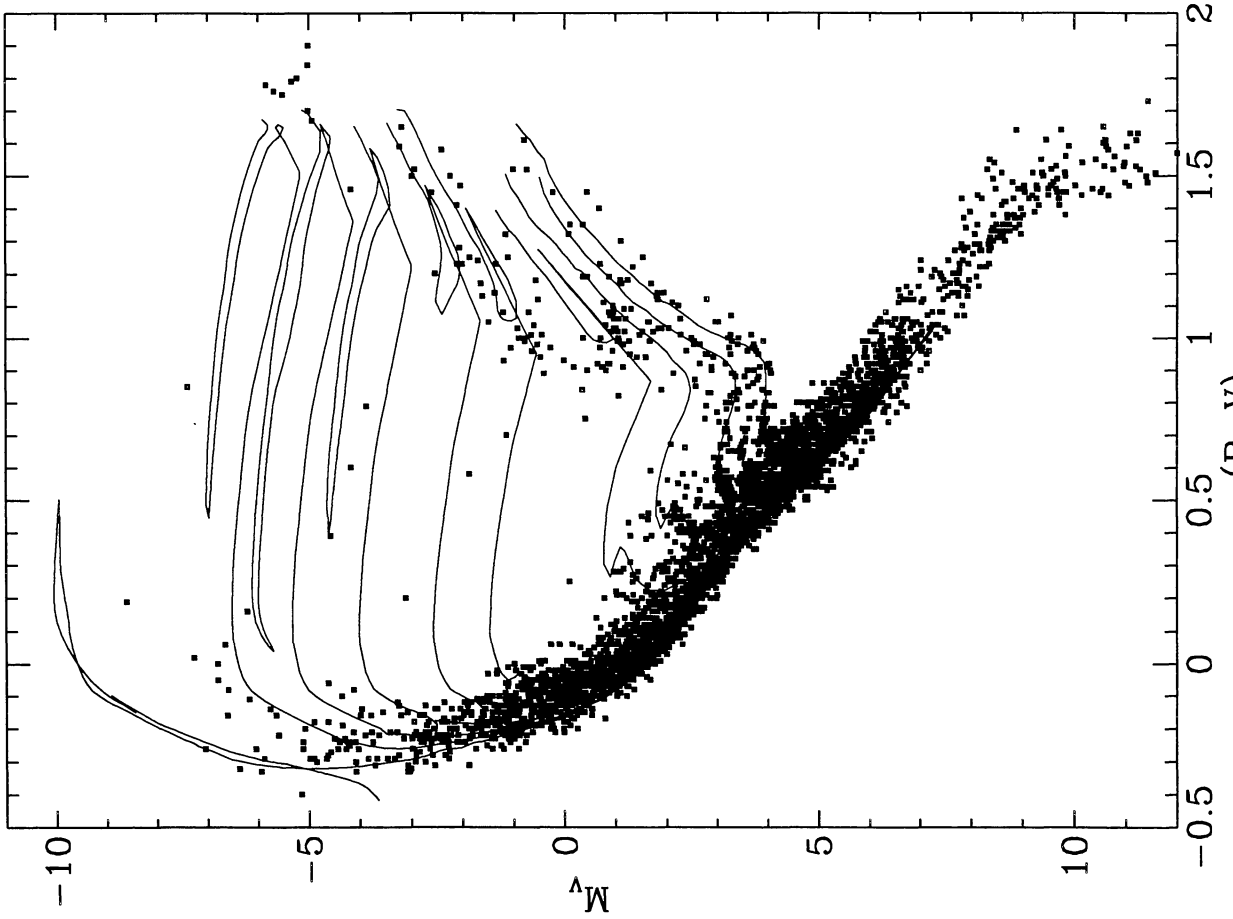

Fig. 6. Synthetic colour-magnitude diagram obtained by the superposition of all the clusters studied in the present work. More than 4000 stars are plotted. A few theoretical isochrones are represented

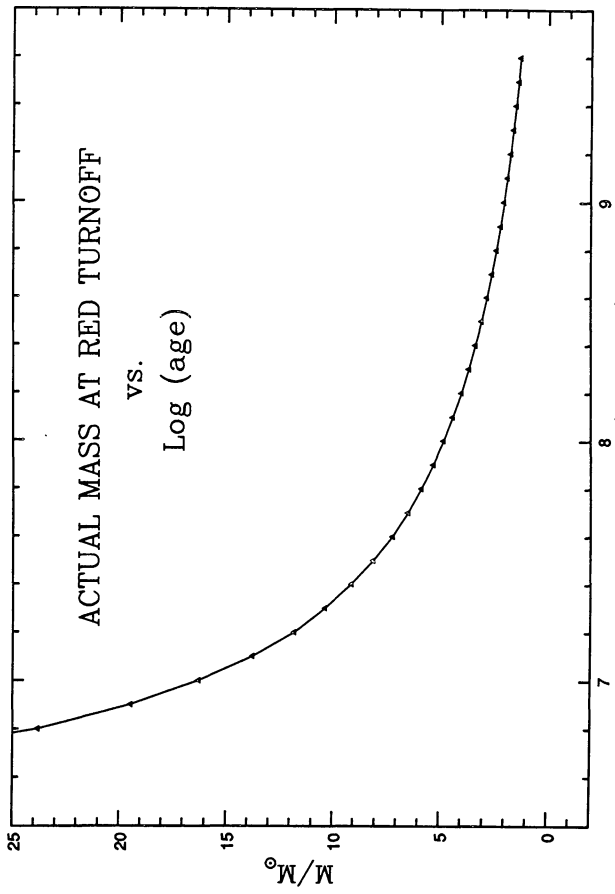

Fig. 5f.

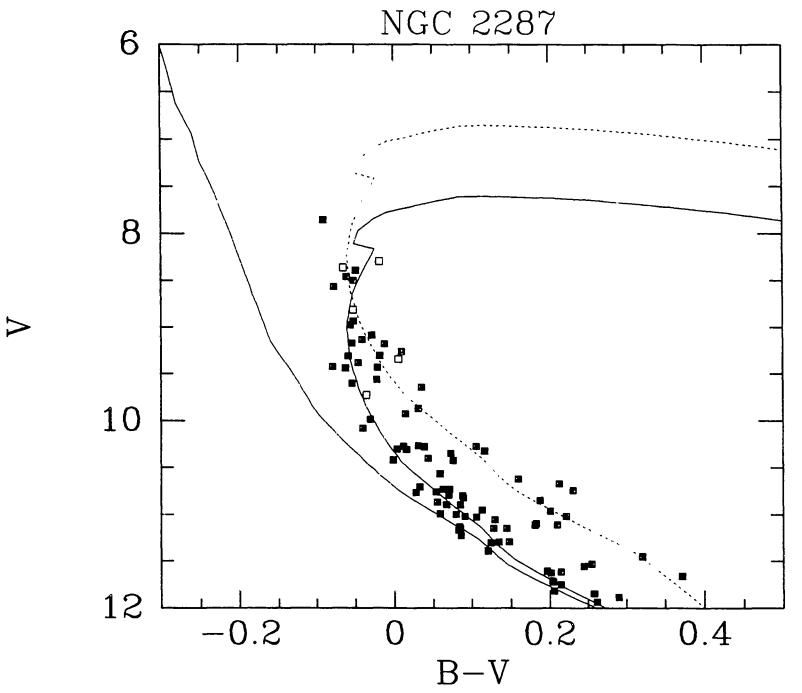

Fig. 7. Fit of an isochrone on the colour magnitude diagram for the open cluster NGC 2287 (V is the apparent visual magnitude). The theoretical envelope for equal mass binaries is also represented. The open squares are identified binaries. The distance modulus, $m - M$, the reddening, $E(B - V)$ and the log *age* are 9.15, 0.01, 8.38 respectively

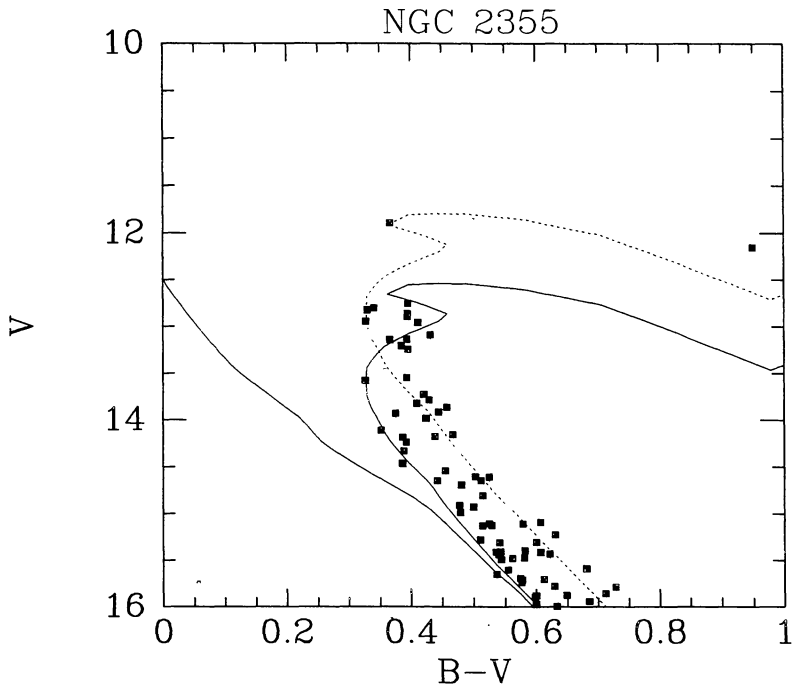

Fig. 8. Same as in Fig. 7 for NGC 2355, $m - M = 11.85$, $E(B - V) = 0.12$, log *age* $= 8.98$

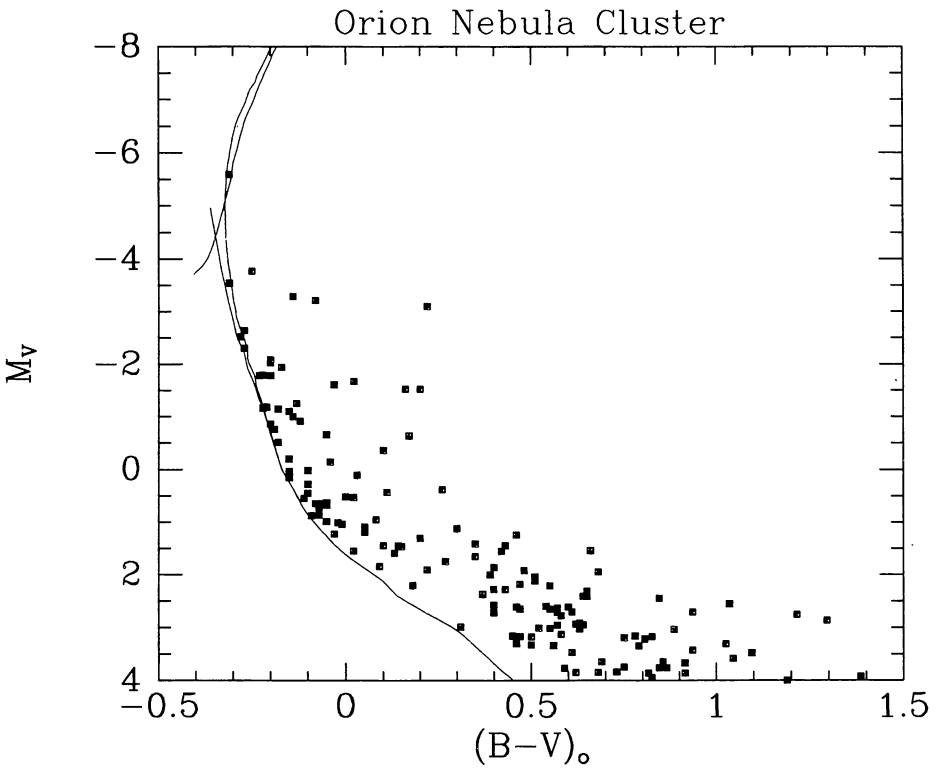

Fig. 9. Fit of an isochrone computed from models with mass loss and overshooting on the colour magnitude diagram for the Orion Nebula cluster (NGC 1976), $m - M = 8.35$, $E(B-V) = 0.05$, log age = 6.60. No corrections for differential reddening have been applied. This explains the anomalous width of the main sequence brighter than $M_v = +1$

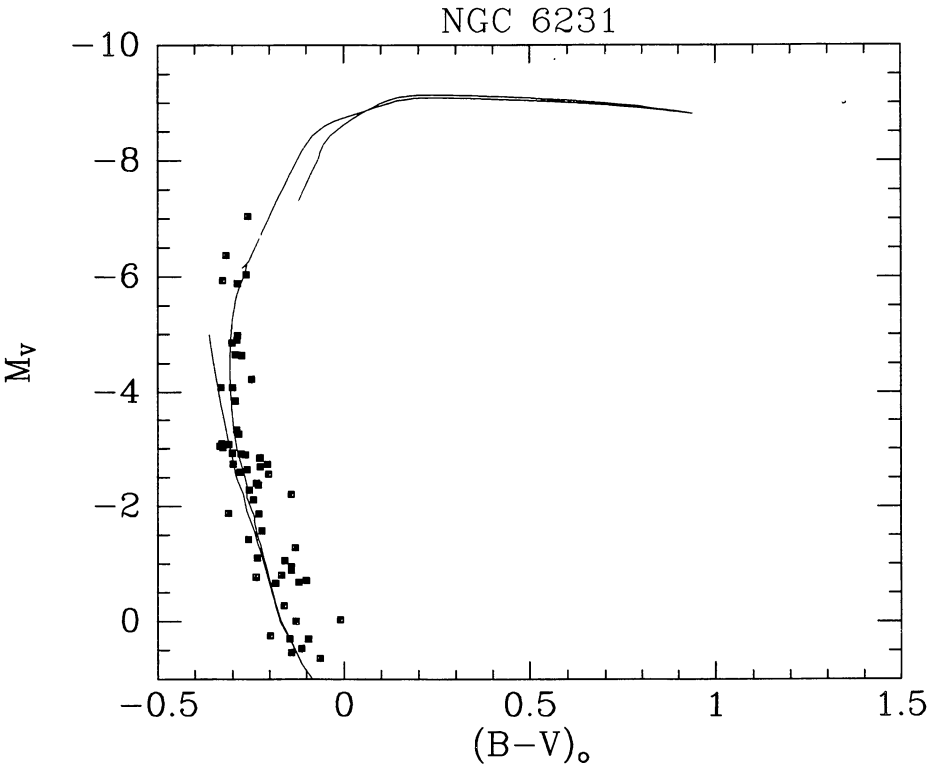

Fig. 10. Same as in Fig. 9 for NGC 6231, $m - M = 12.50$, $E(B-V) = 0.46$, log $age = 6.75$

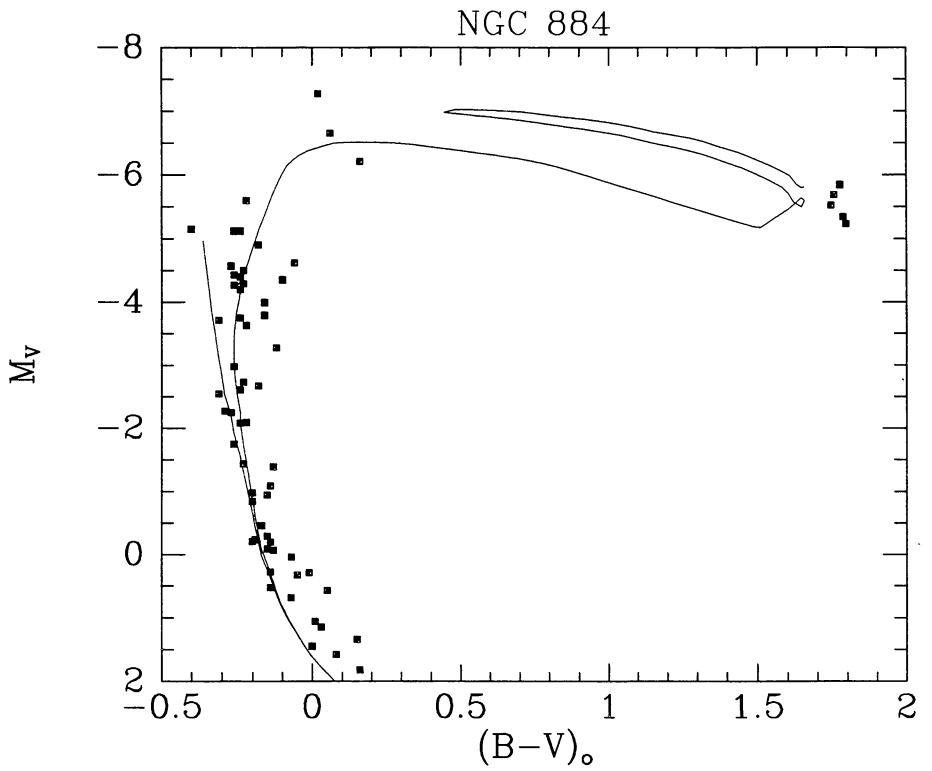

Fig. 11. Same as in Fig. 9 for NGC 884, $m - M = 13.65$, $E(B - V) = 0.56$, log $age = 7.15$. The scatter around the main sequence is due to the presence of numerous Be stars

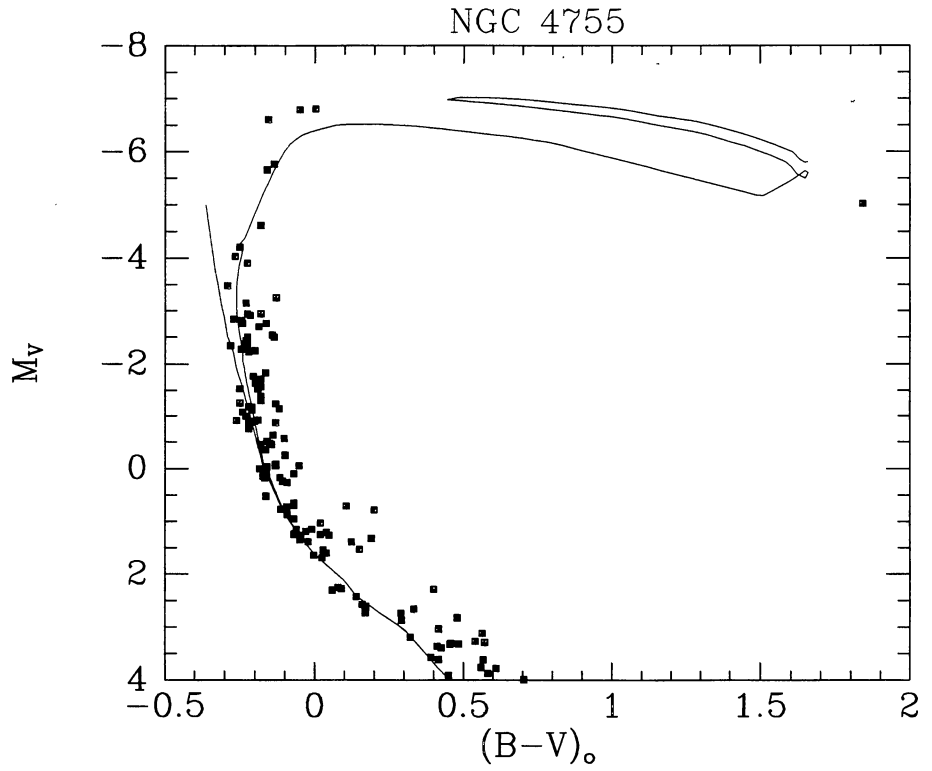

Fig. 12. Same as in Fig. 9 for NGC 4755, $m - M = 12.55$, $E(B - V) = 0.38$, log $age = 7.15$

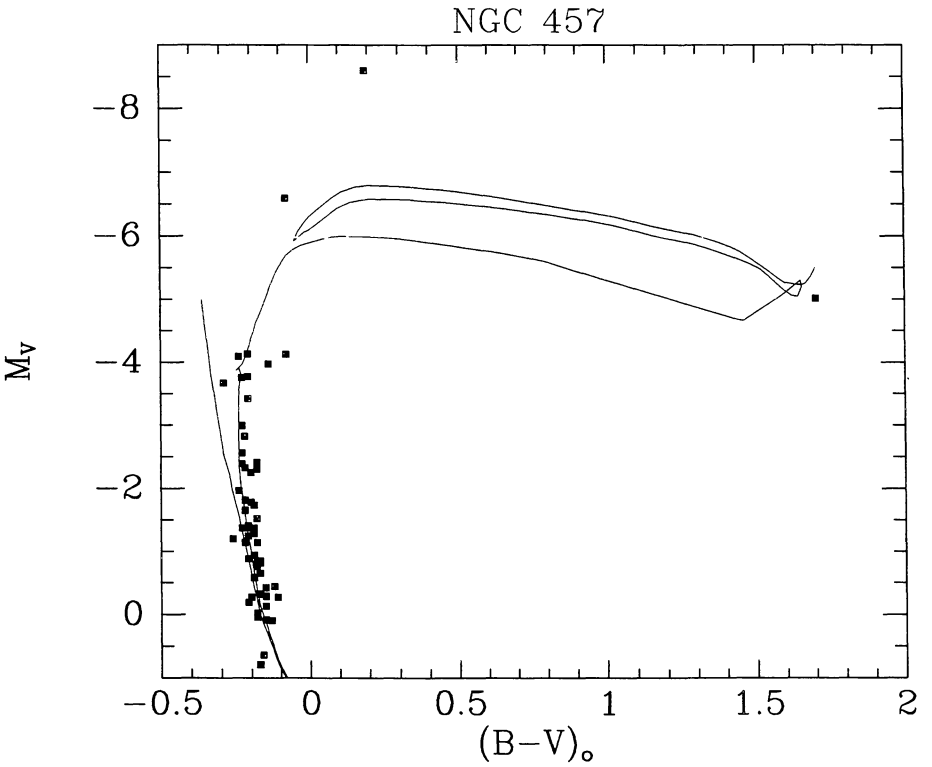

Fig. 13. Same as in Fig. 9 for NGC 457, $m - M = 13.60$, $E(B - V) = 0.50$, log *age* = 7.25. The isochrone gives a good description of the red and blue supergiants

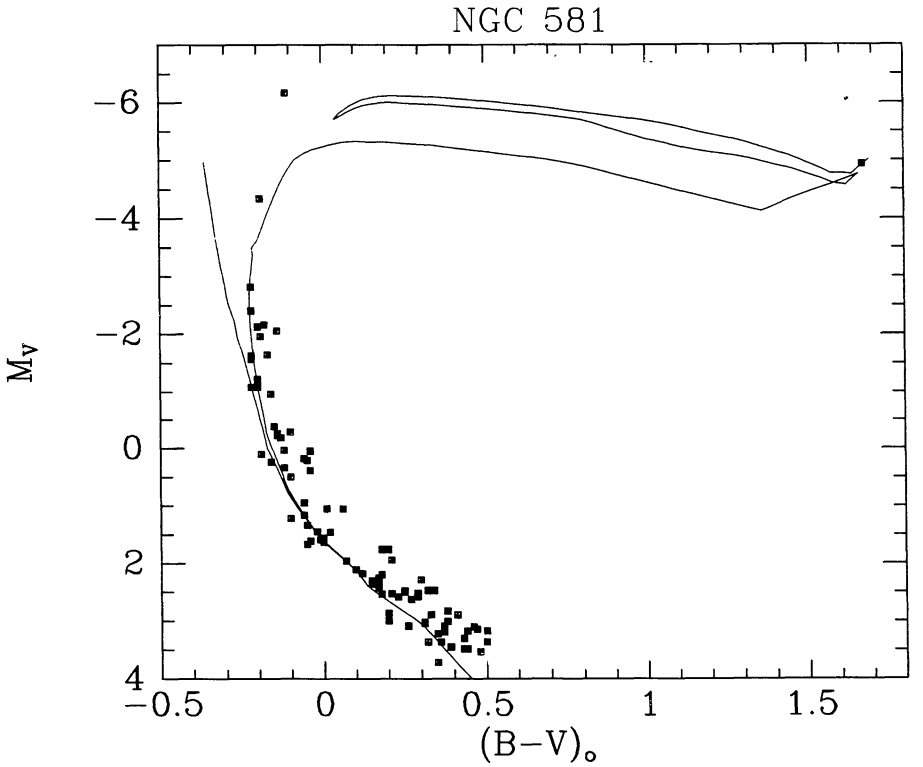

Fig. 14. Same as in Fig. 9 for NGC 581, $m - M = 13.26$, $E(B - V) = 0.40$, log *age* = 7.40. Same comments as in Fig. 13

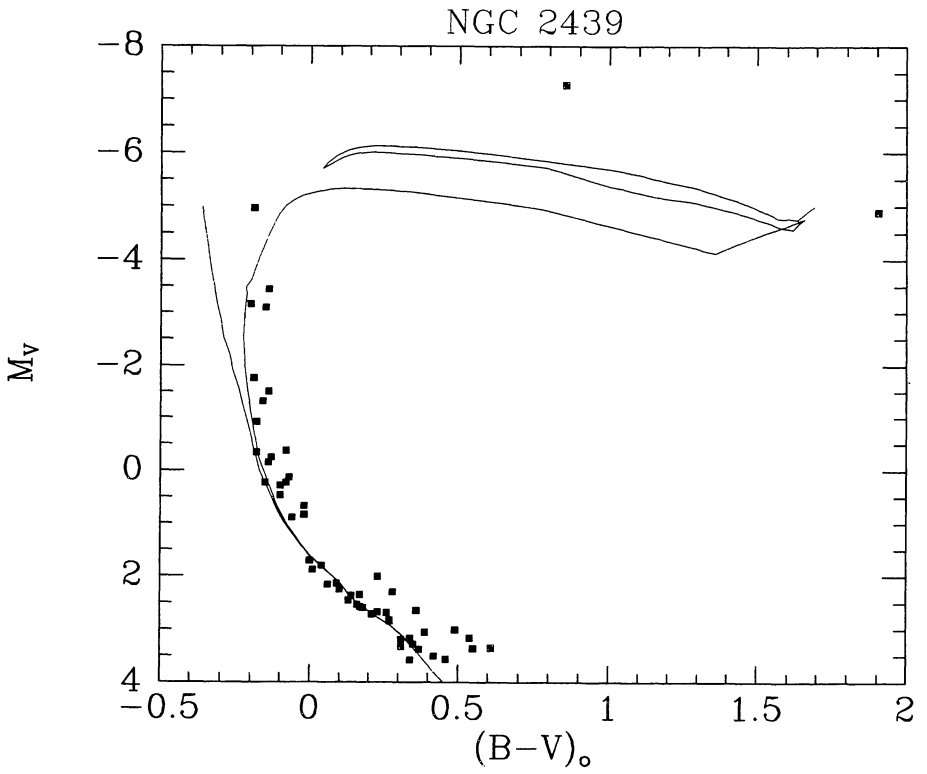

Fig. 15. Same as in Fig. 9 for NGC 2439, $m - M = 14.00$, $E(B - V) = 0.36$, log $age = 7.40$

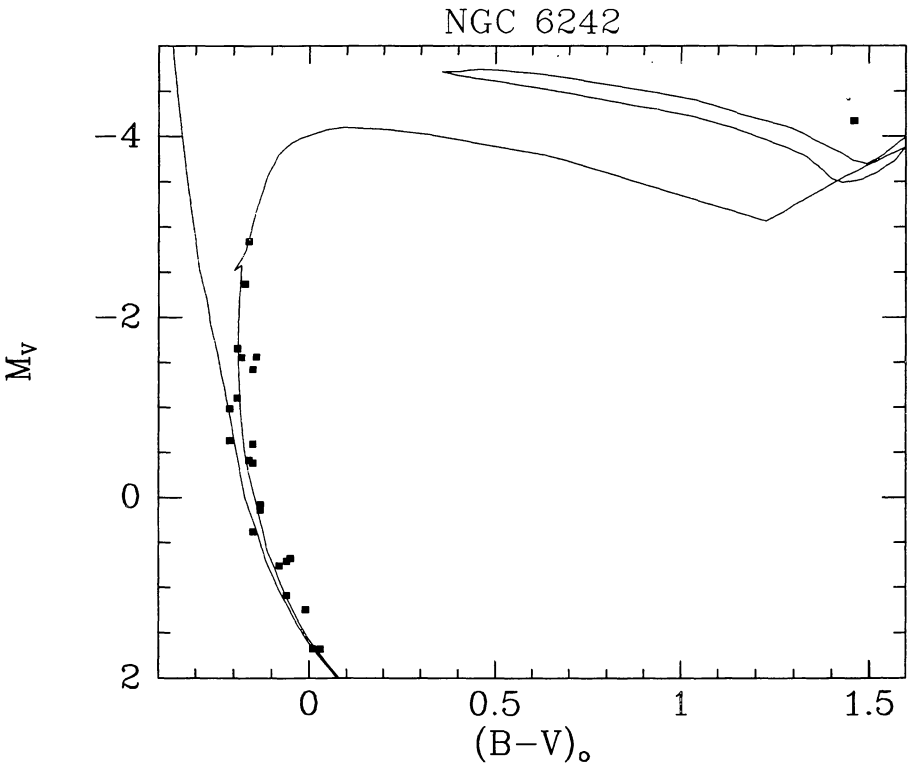

Fig. 16. Same as in Fig. 9 for NGC 6242, $m - M = 11.45$, $E(B - V) = 0.39$, log $age = 7.70$

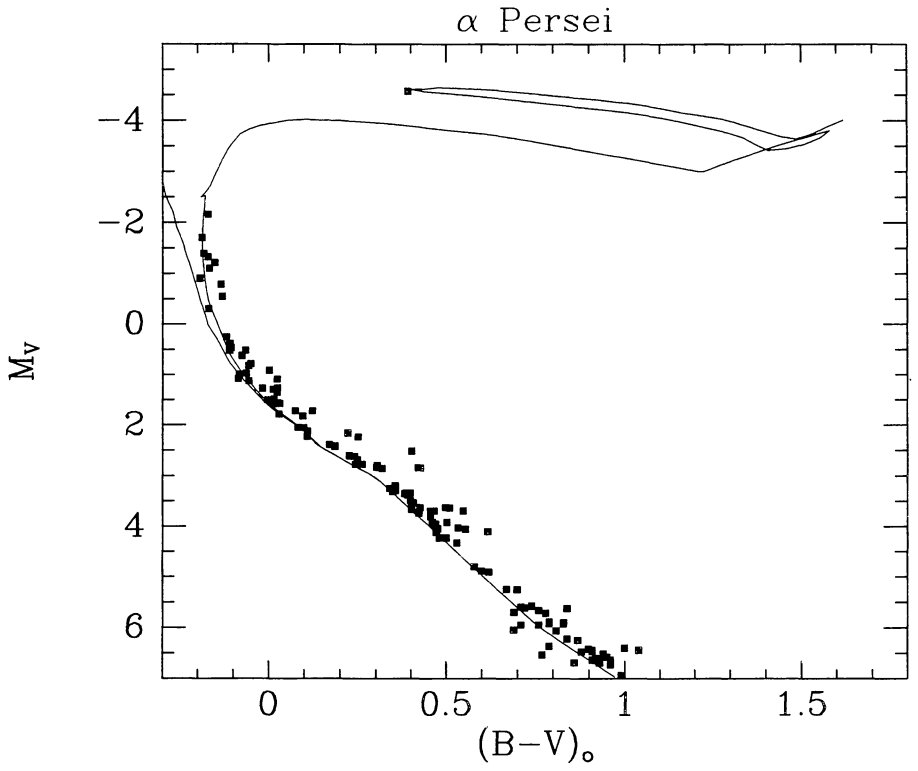

Fig. 17. Same as in Fig. 9 for α Persei, $m - M = 6.36$, $E(B-V) = 0.09$, log *age* = 7.72. The isochrone perfectly fits simultaneously the MS shape and the position of the yellow supergiant, α Per itself

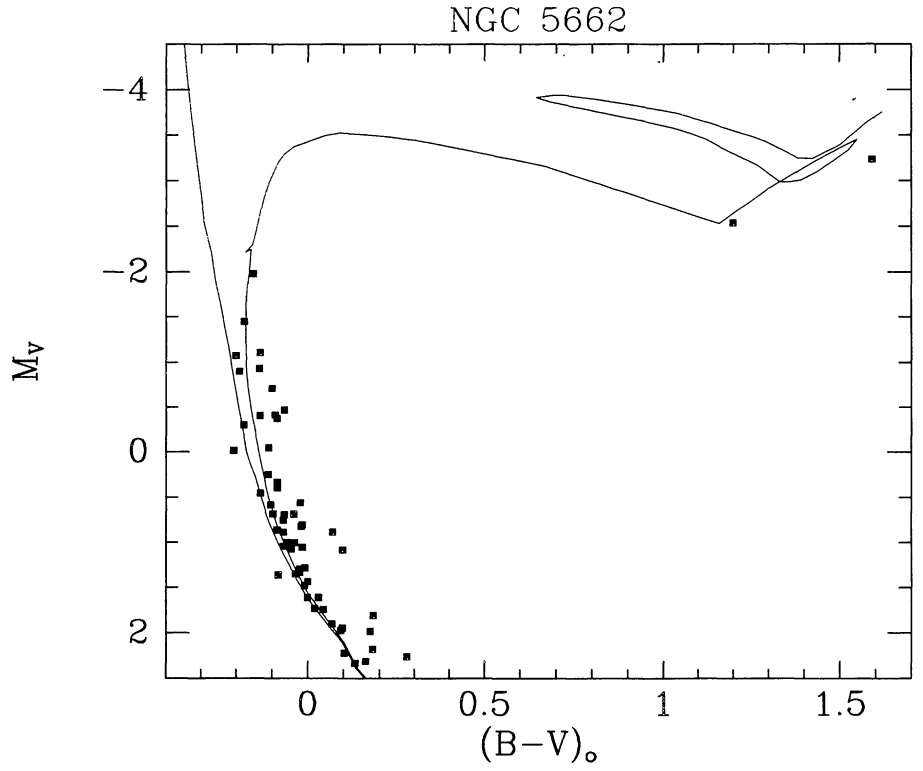

Fig. 18. Same as in Fig. 9 for NGC 5662, $m - M = 10.30$, $E(B-V) = 0.31$, log *age* = 7.85

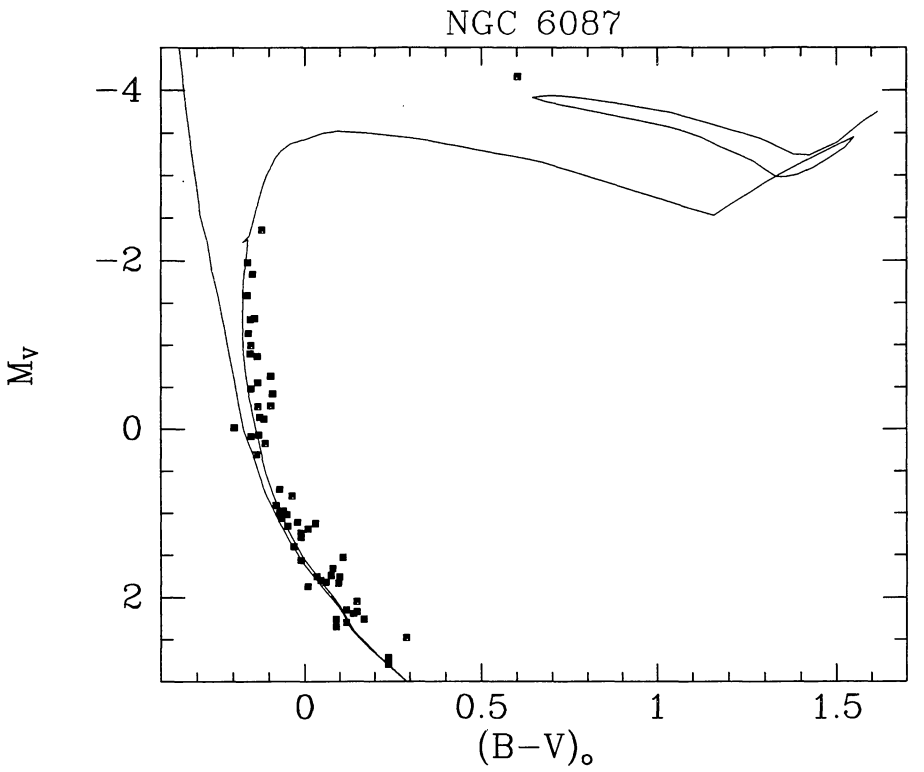

Fig. 19. Same as in Fig. 9 for NGC 6087, $m - M = 10.30$, $E(B - V) = 0.20$, log $age = 7.85$

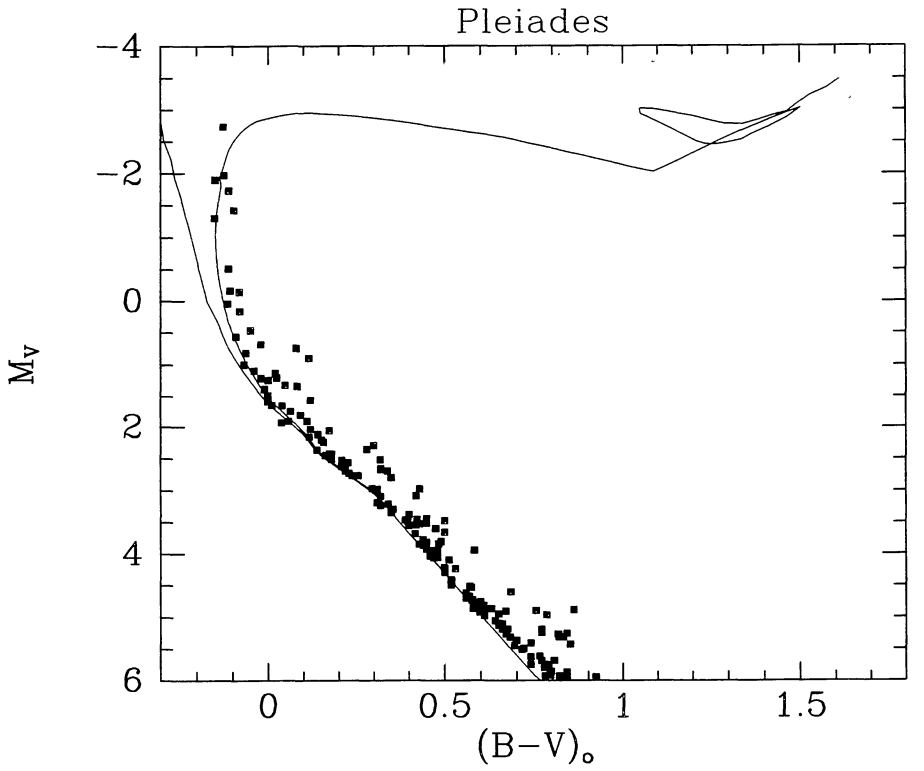

Fig. 20. Same as in Fig. 9 for the Pleiades, $m - M = 5.60$, $E(B - V) = 0.04$, log $age = 8.00$

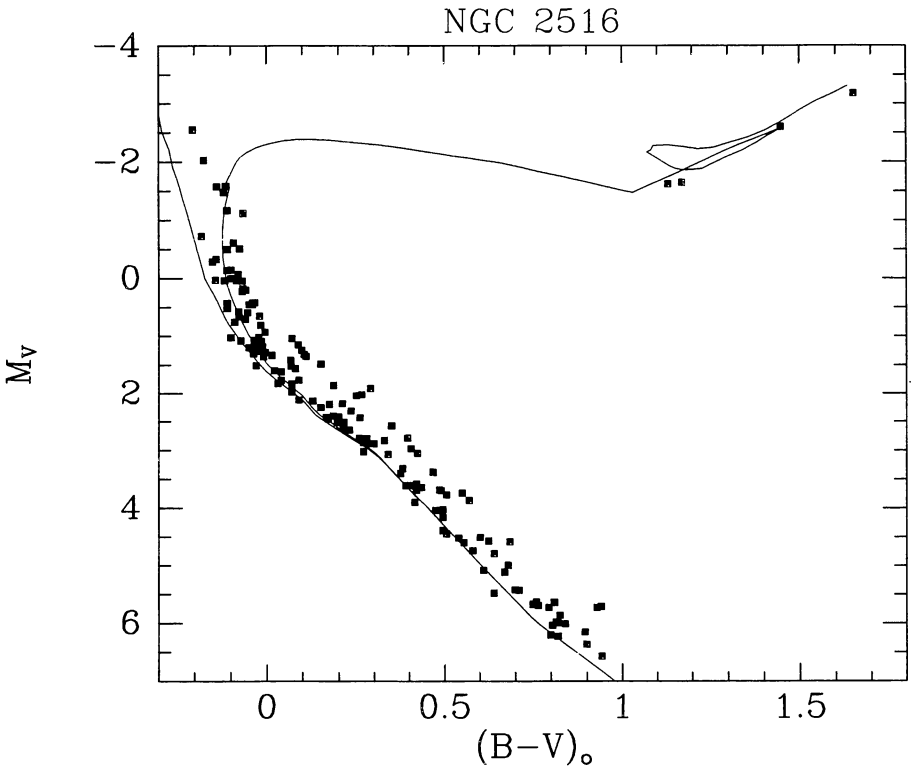

Fig. 21. Same as in Fig. 9 for NGC 2516, $m - M = 8.35$, $E(B - V) = 0.12$, log $age = 8.15$

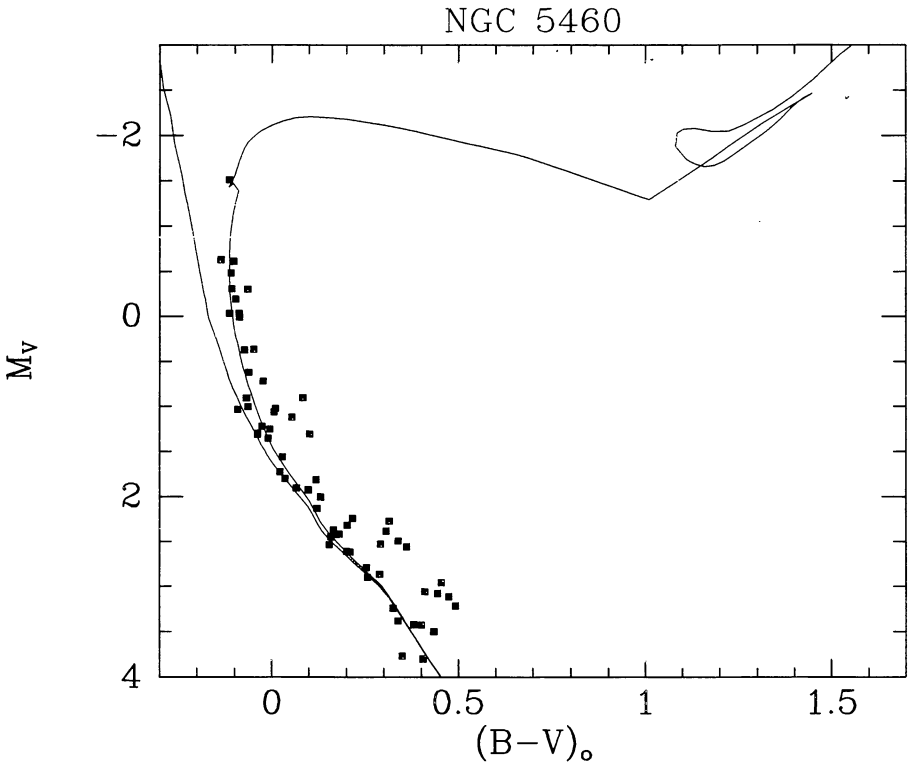

Fig. 22. Same as in Fig. 9 for NGC 5460, $m - M = 9.50$, $E(B - V) = 0.12$, log $age = 8.20$

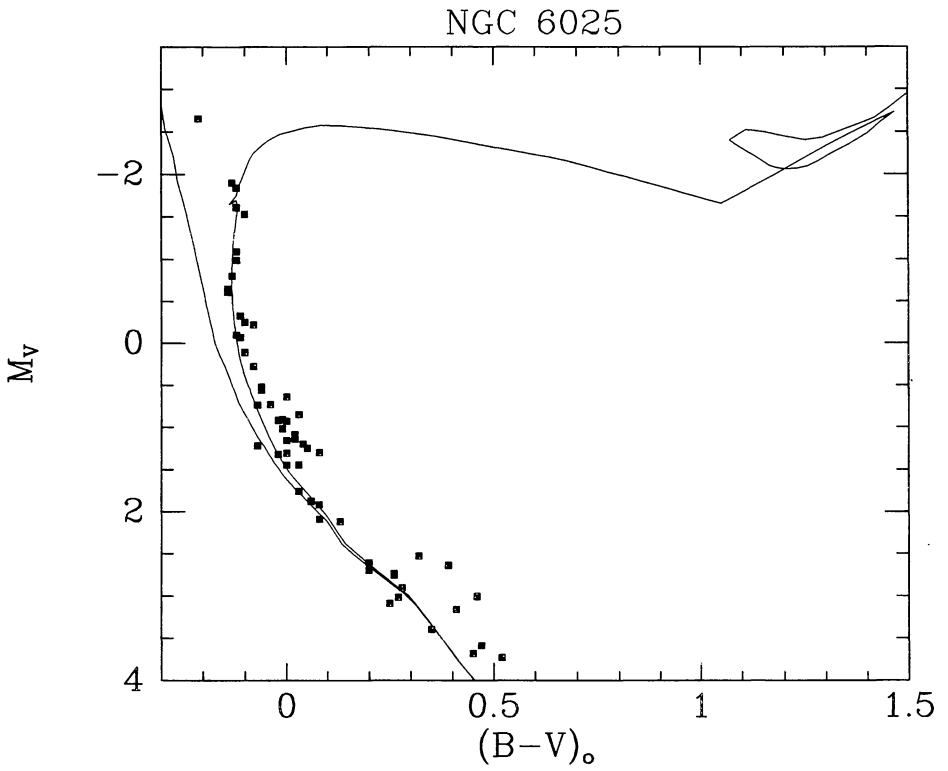

Fig. 23. Same as in Fig. 9 for NGC 6025, $m - M = 9.95$, $E(B - V) = 0.16$, log $age = 8.10$

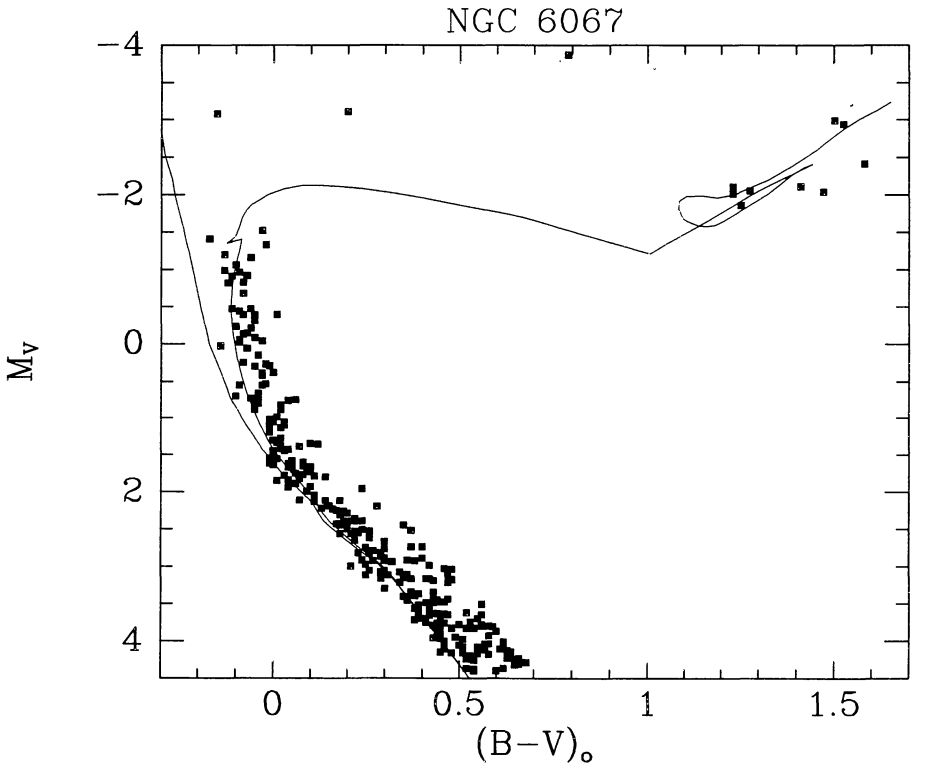

Fig. 24. Same as in Fig. 9 for NGC 6067, $m - M = 12.10$, $E(B - V) = 0.32$, log $age = 8.22$

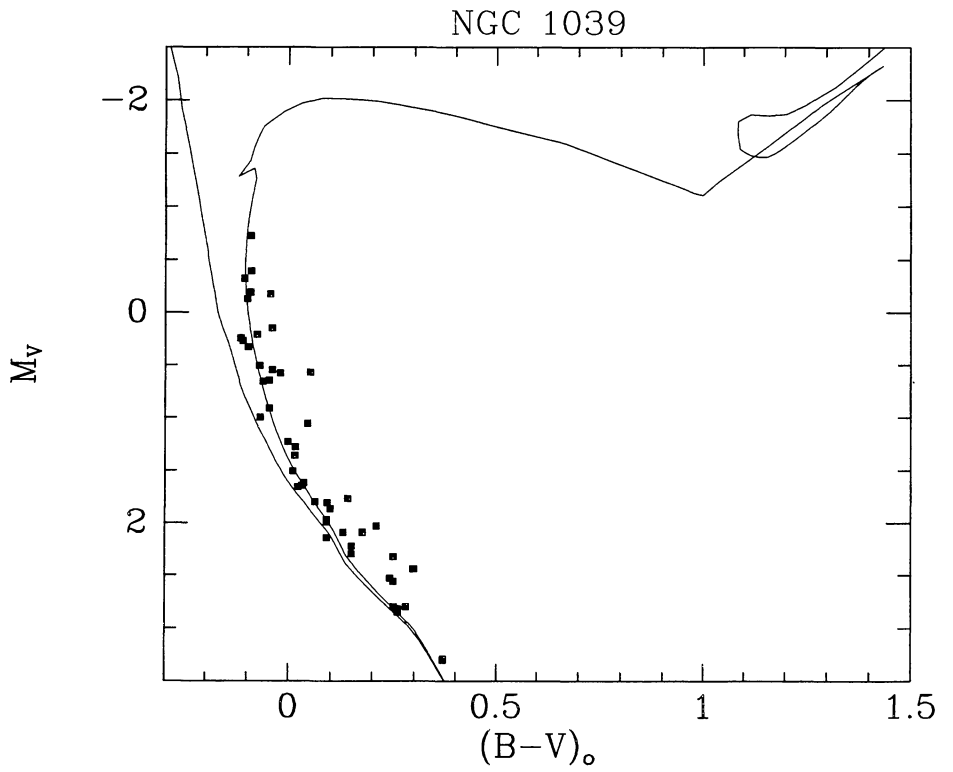

Fig. 25. Same as in Fig. 9 for NGC 1039, $m - M = 8.65$, $E(B - V) = 0.10$, log $age = 8.25$

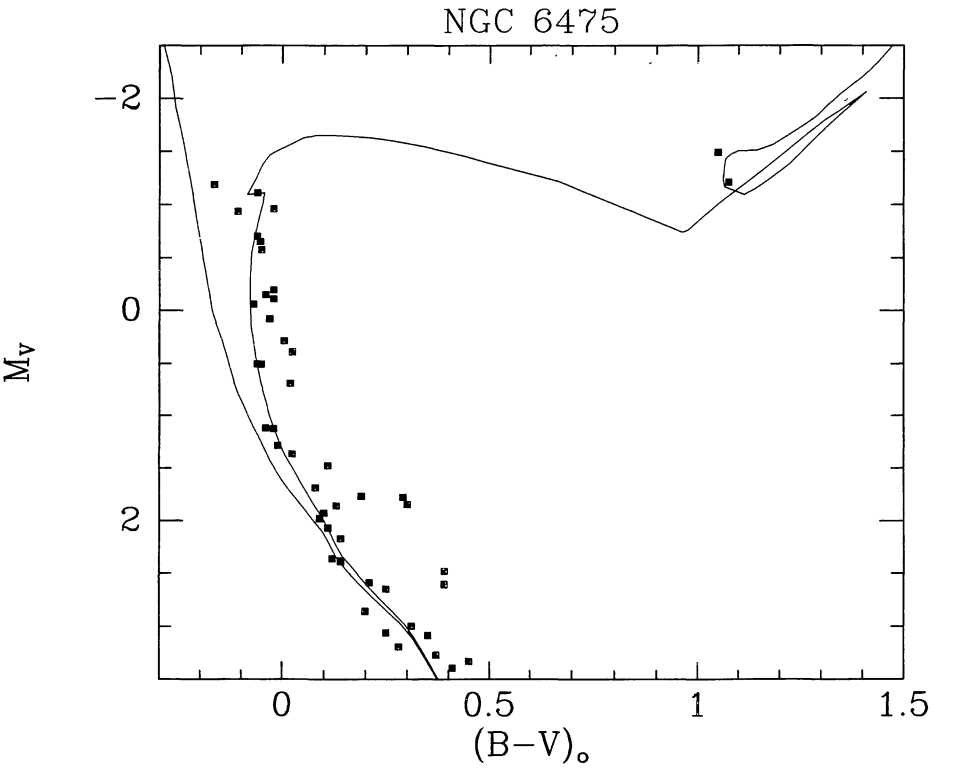

Fig. 26. Same as in Fig. 9 for NGC 6475, $m - M = 7.08$, $E(B - V) = 0.06$, log $age = 8.35$

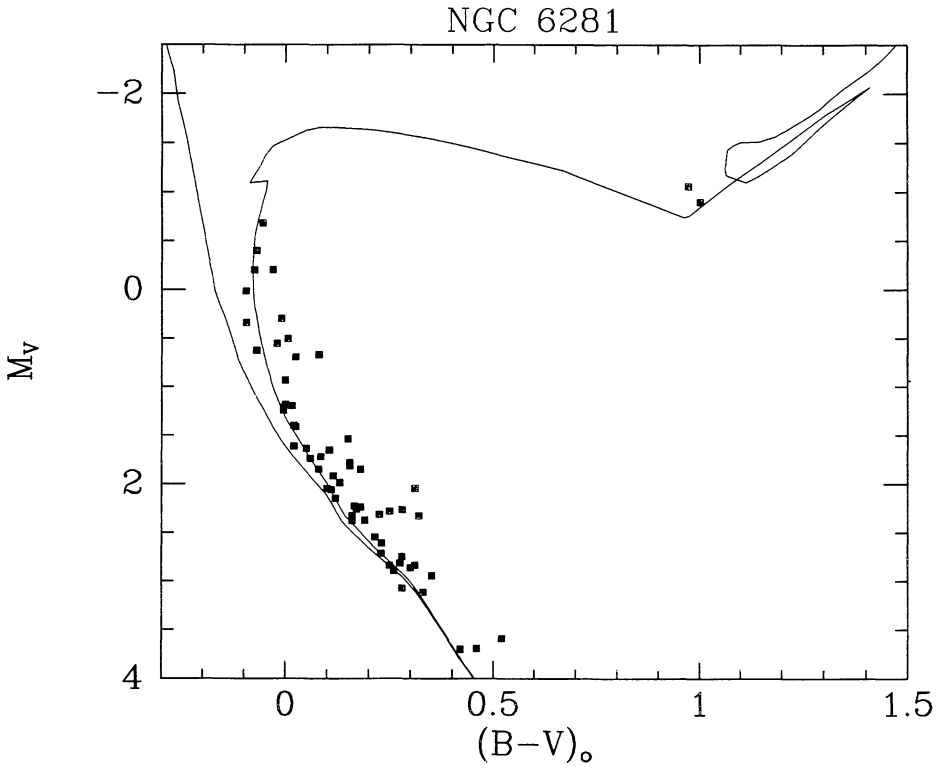

Fig. 27. Same as in Fig. 9 for NGC 6281, $m - M = 9.00$, $E(B - V) = 0.16$, log $age = 8.35$

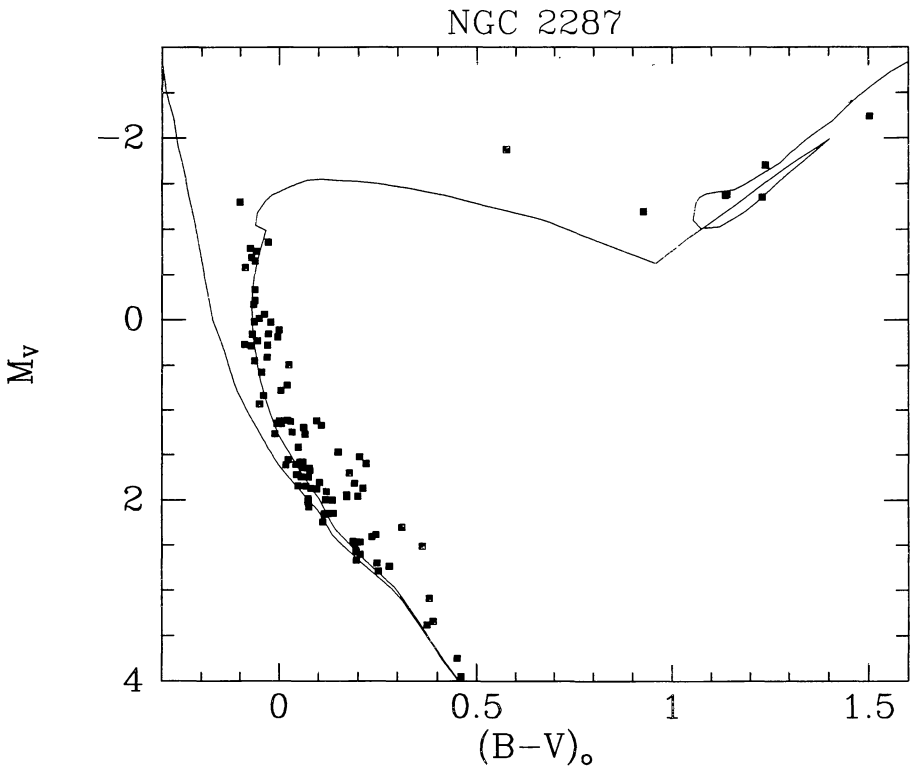

Fig. 28. Same as in Fig. 9 for NGC 2287, $m - M = 9.15$, $E(B - V) = 0.01$, log $age = 8.38$

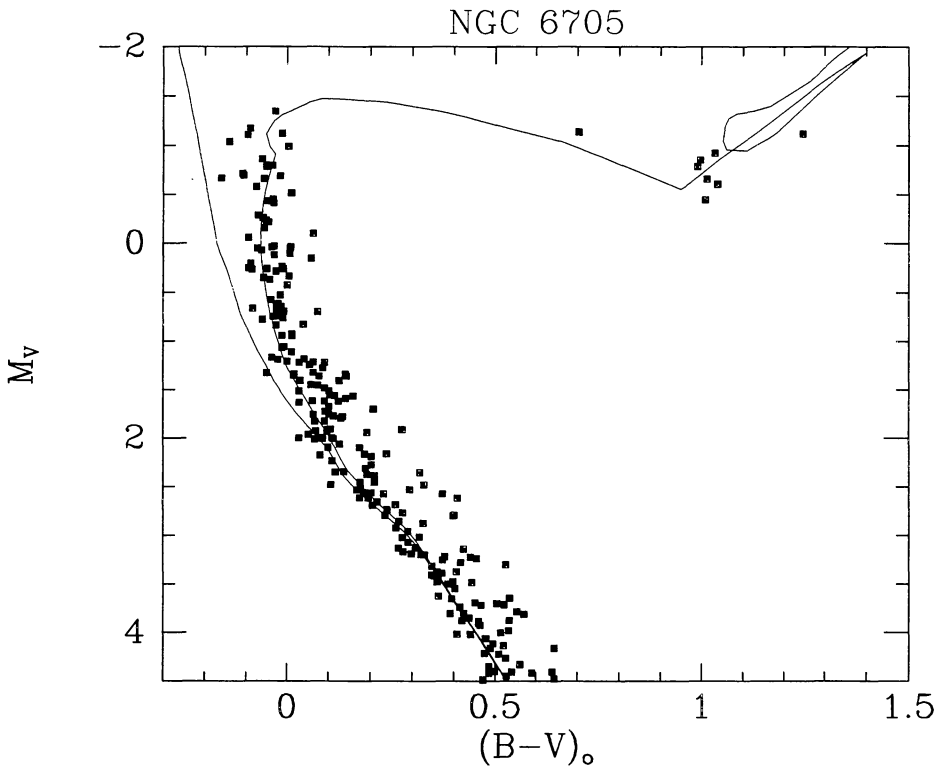

Fig. 29. Same as in Fig. 9 for NGC 6705, $m - M = 12.70$, $E(B-V) = 0.40$, log $age = 8.40$

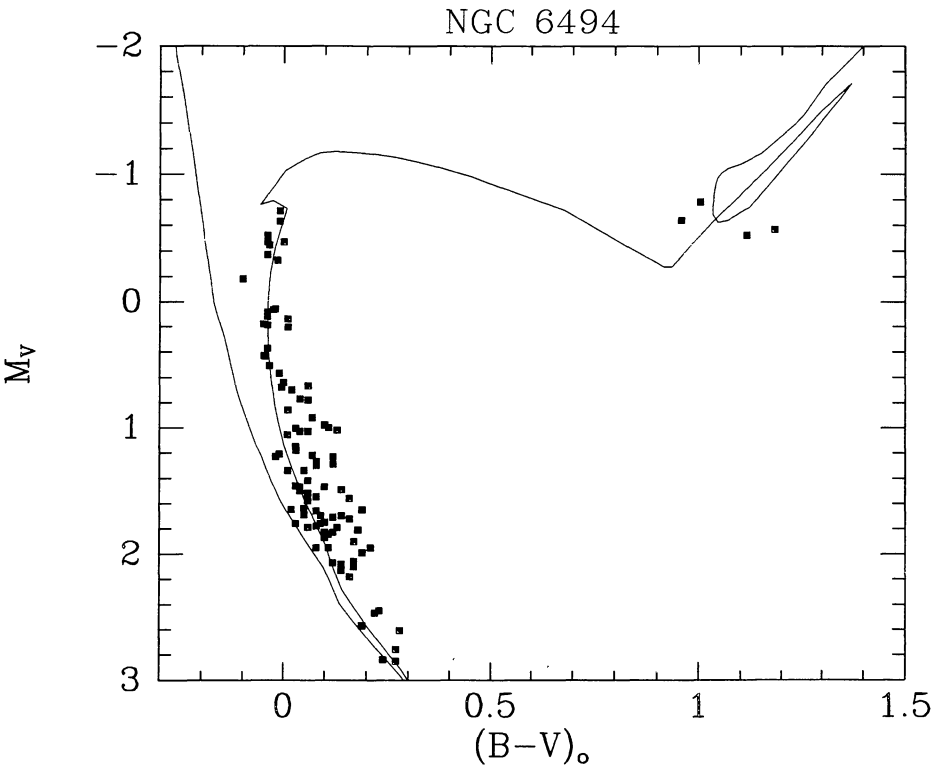

Fig. 30. Same as in Fig. 9 for NGC 6494, $m - M = 10.20$, $E(B-V) = 0.36$, log $age = 8.48$

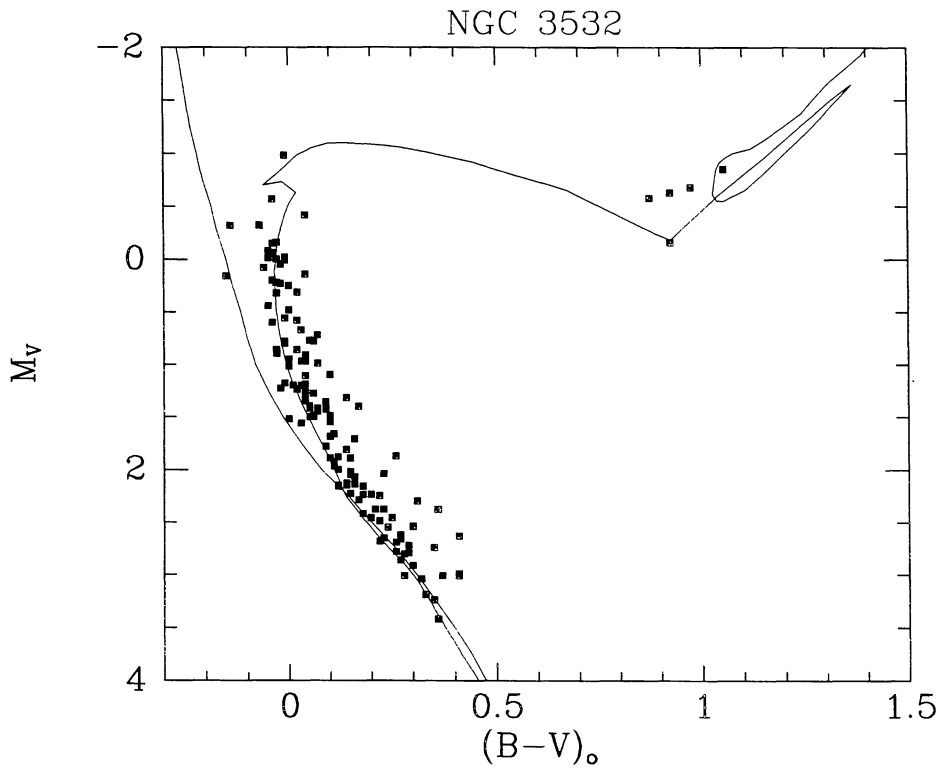

Fig. 31. Same as in Fig. 9 for NGC 3532, $m - M = 8.35$, $E(B - V) = 0.04$, log $age = 8.50$

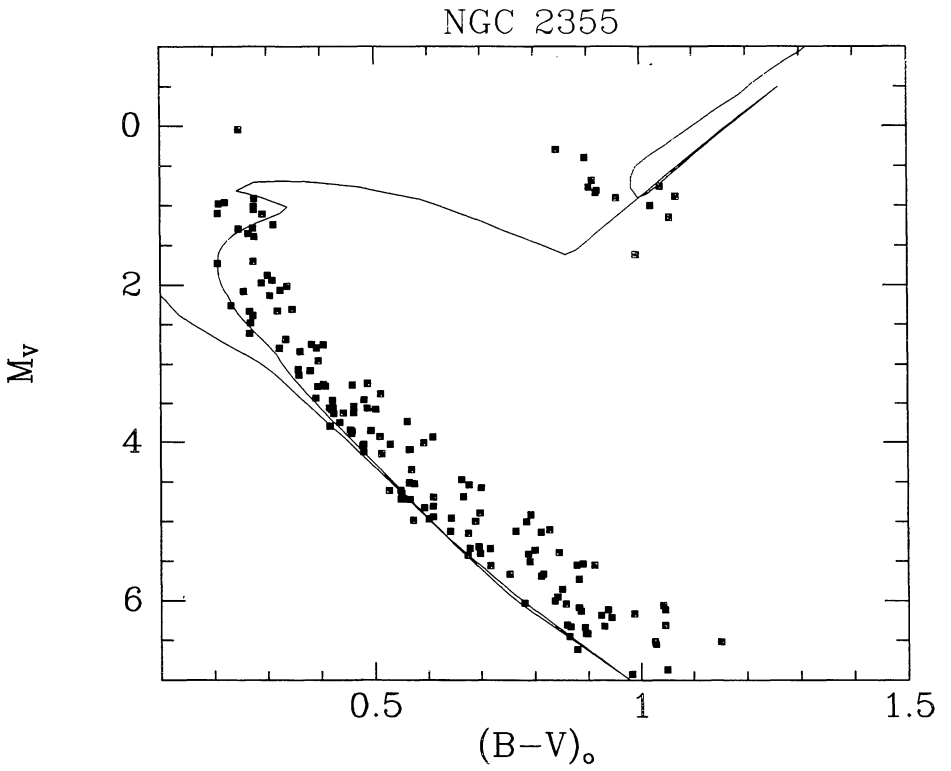

Fig. 32. Same as in Fig. 9 for NGC 2355, $m - M = 11.85$, $E(B - V) = 0.12$, log $age = 8.98$. See Fig. 8 for the interpretation of the upper main sequence

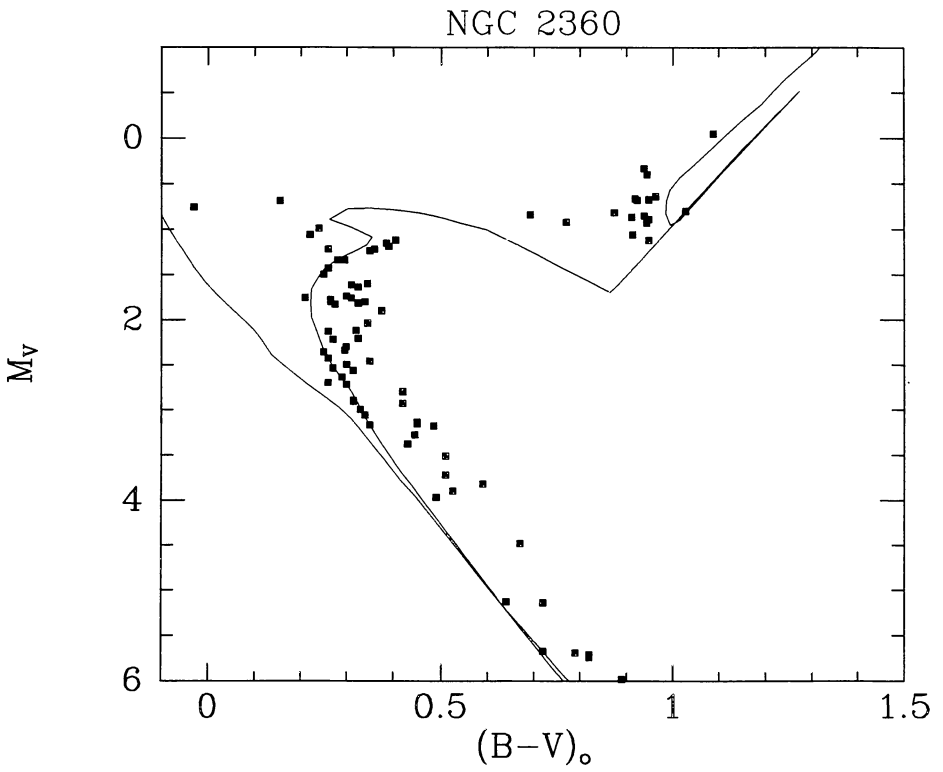

Fig. 33. Same as in Fig. 9 for NGC 2360, $m - M = 10.40$, $E(B-V) = 0.08$, log *age* = 9.00. The isochrone reproduces very well the shape of the main sequence, which seems to extend even more redwards

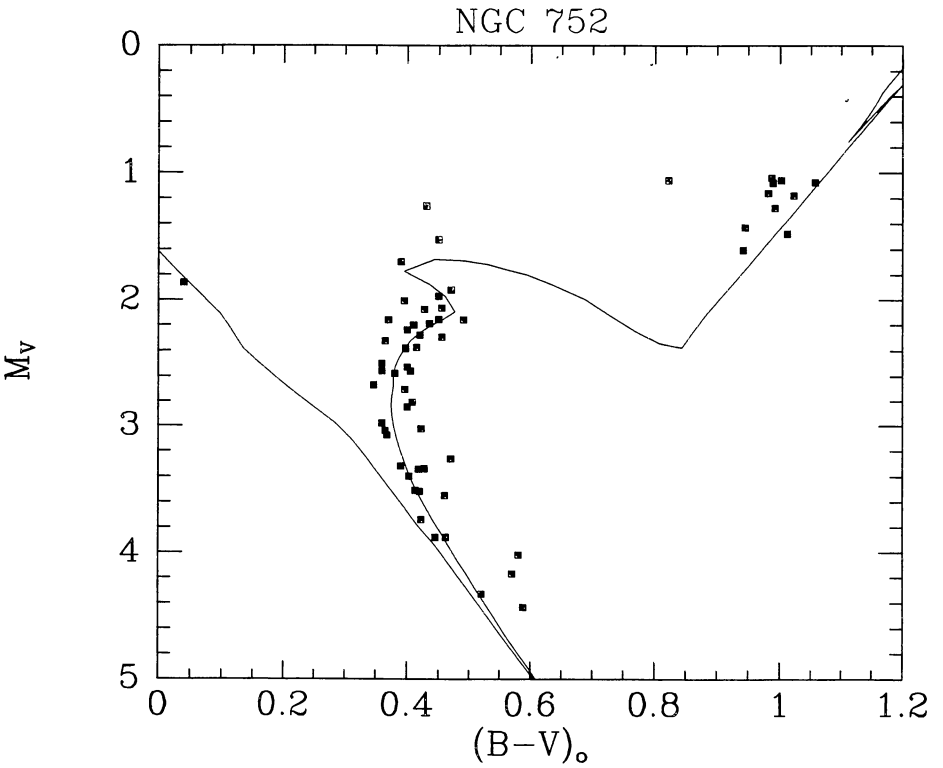

Fig. 34. Same as in Fig. 9 for NGC 752, $m - M = 7.88$, $E(B-V) = 0.02$, log *age* = 9.25. The isochrone reproduces well the extension of the main sequence when one allows correctly for the binarity effect

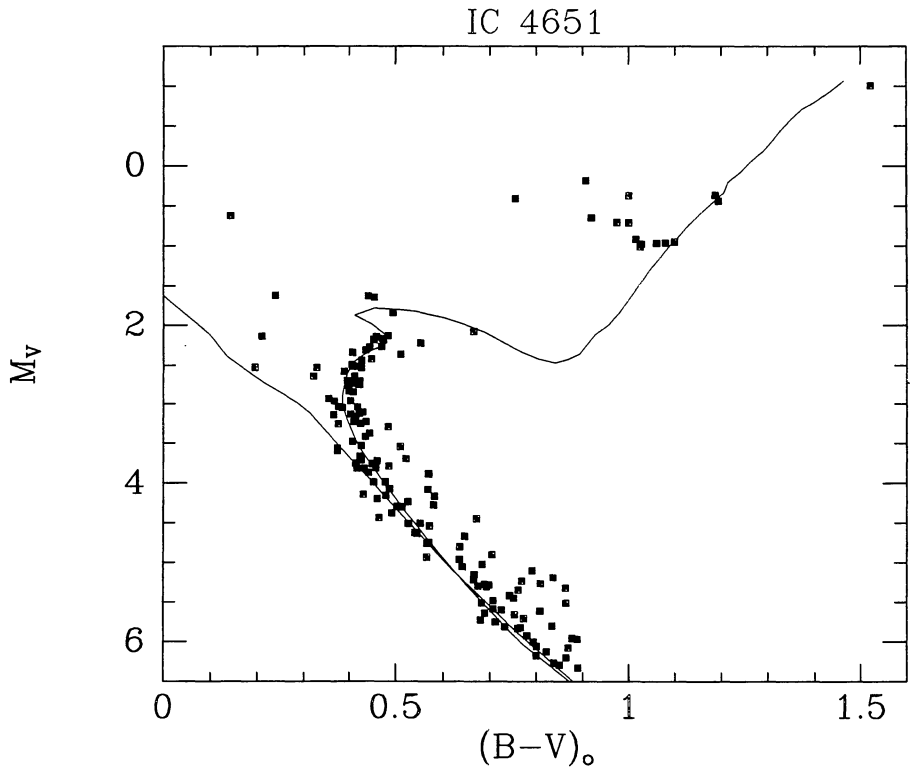

Fig. 35. Same as in Fig. 9 for IC 4651, $m - M = 9.90$, $E(B - V) = 0.14$, log *age* = 9.28. This is the only diagram based on photographic data. The scatter is nevertheless very small and the fit of the isochrone pretty good

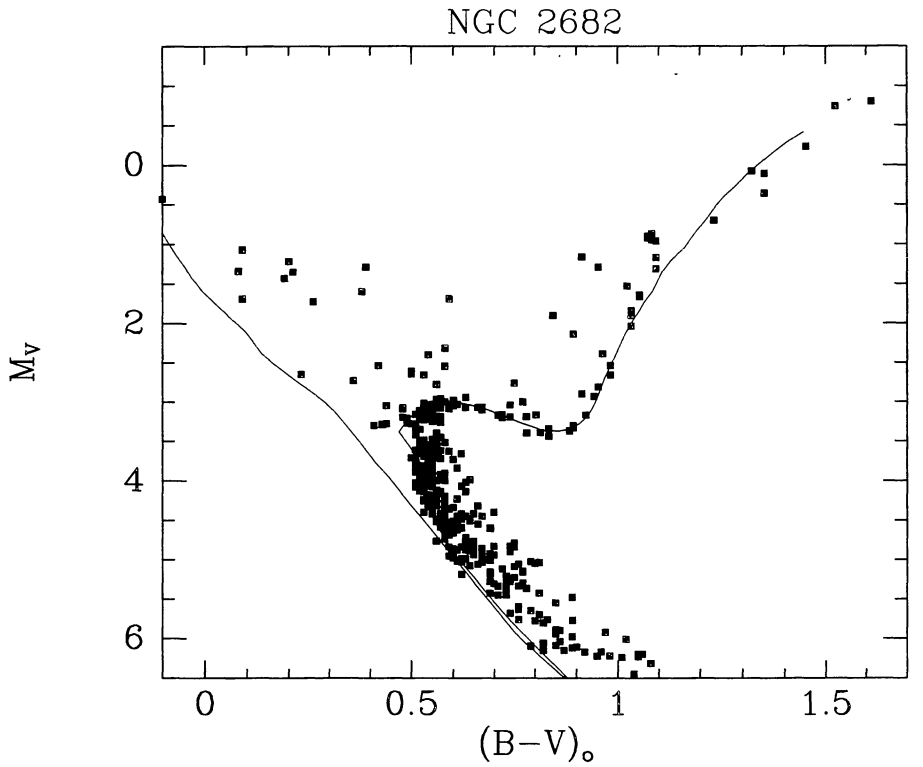

Fig. 36. Fit of an isochrone computed from models without overshooting on the colour-magnitude diagram for NGC 2682, $m - M = 9.60$, $E(B - V) = 0.03$, log *age* = 9.60. This combination of parameters suggested by Twarog and Anthony-Twarog (1988) is the only one which produces a good fit

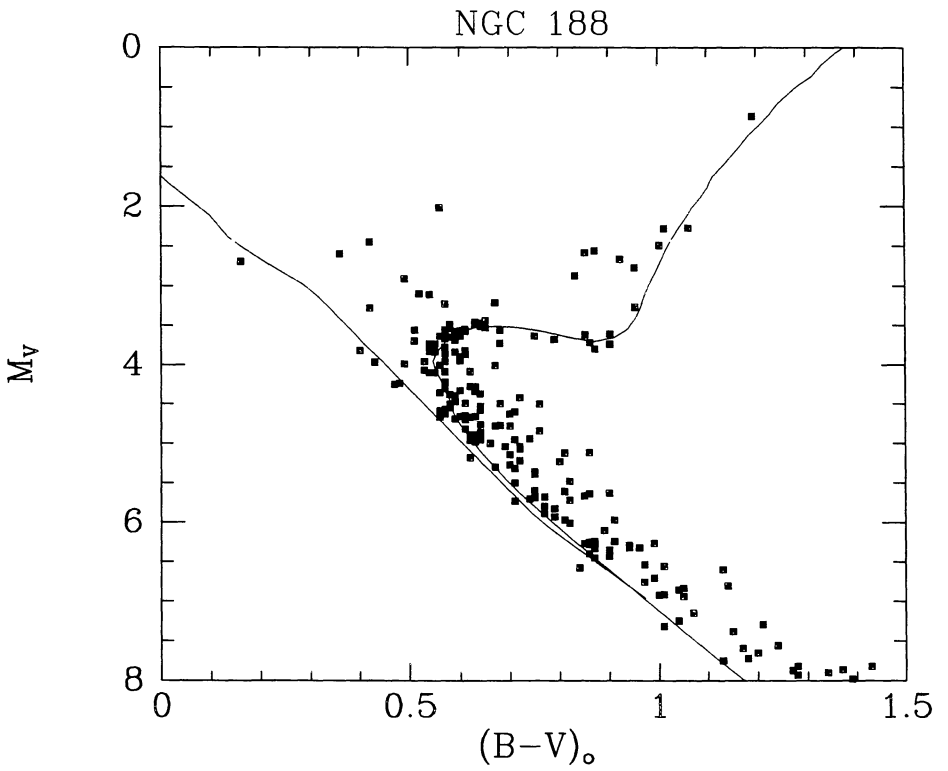

Fig. 37. Same as in Fig. 36 for NGC 188, $m - M = 11.35$, $E(B - V) = 0.12$, log $age = 9.82$. Same comments as for Fig. 36

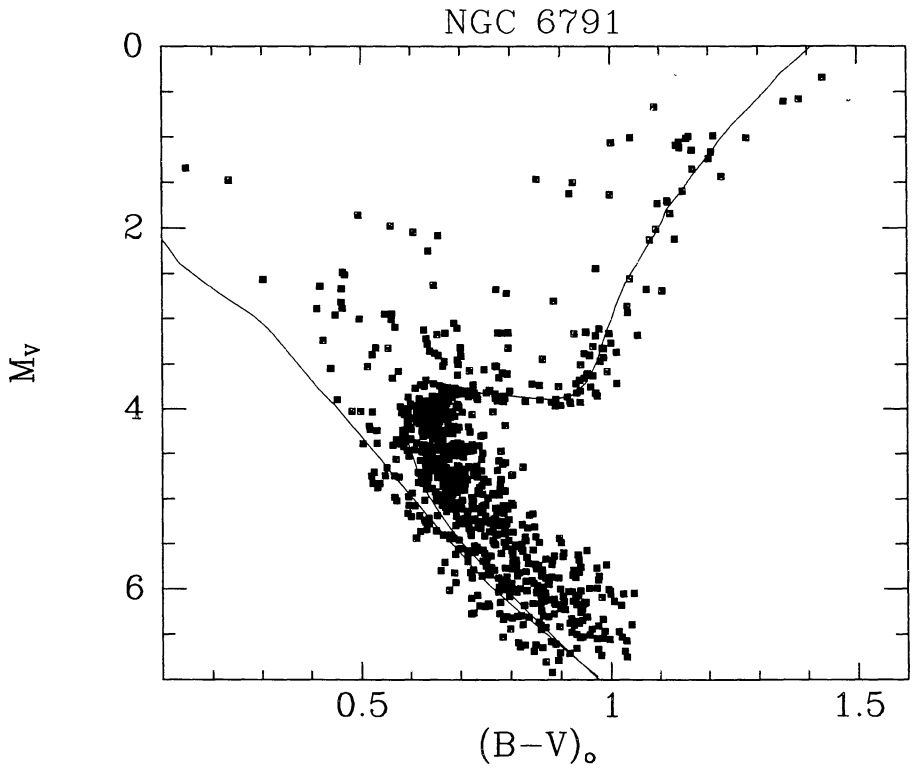

Fig. 38. Same as in Fig. 36 for NGC 6791, $m - M = 13.55$, $E(B - V) = 0.21$, log $age = 9.95$. The star membership to this cluster is not well defined from only the photometric analysis, which explains the poor definition of the main sequence limits